DESIGN AND OPTIMIZATION OF QCM BIOSENSOR TO DETECT MALIGNANT MELANOMA CELLS VIA THEIR CD44 RECEPTORS

MALİN MELANOMA HÜCRELERİNİ CD44 RESEPTÖRLERİ ARACILIĞIYLA TANIMLAYAN QCM SENSÖR TASARIMI VE OPTİMİZASYONU

RAHAF SAMEER TAOFEK AIOSH

ASSOC. PROF. DR. ERDOĞAN ÖZGÜR
Supervisor

Graduate School of Science and Engineering of Hacettepe University
As a partial Fulfillment to the Requirements
For the Award of the Degree of Master of Science
In Chemistry

2024

I dedicate my master's thesis to the souls of my dear grandfather and grandmother, whom I lost to cancer, and to all cancer fighters around the world.

ÖZET

MALİN MELANOMA HÜCRELERİNİ CD44 RESEPTÖRLERİ ARACILIĞIYLA TANIMLAYAN QCM SENSÖR TASARIMI VE OPTİMİZASYONU

Rahaf Sameer Taofek AIOSH

Yüksek Lisans, Kimya Bölümü

Tez Danışmanı: Doç. Dr. Erdoğan ÖZGÜR

Haziran 2024, 86 sayfa

Malign melanom (MM), melanositlerden köken alan deri kanserinin son derece agresif bir formudur ve küresel olarak önemli bir halk sağlığı sorunu olarak ortaya çıkmaktadır. Artan insidansı ve metastaz eğilimi, erken teşhis ve müdahaleyi mümkün kılacak yenilikçi tanı yaklaşımlarına olan kritik ihtiyacı vurgulamaktadır. Bu tezde, MM hücrelerini CD44 (kümeleme farklılaşma 44) reseptörleri aracılığıyla tespit etme yeteneğine sahip bir kuvars kristal dengesi (QCM) biyosensörünün tasarımı ve optimize edilmesini önererek, bu acil sorunu ele almaktayız. MM hücrelerinin yüzeylerinde çok yüksek düzeyde ifade edilir. Bu hücreleri tanımlamayı, QCM'i DF6392 adlı CD44 bağlayıcı antikor ile birleştirerek amaçladık. İlk adımda, QCM çipinin yüzey alanını arttırmak için, 2-hidroksietil metakril (HEMA) ve etilen glikoldimetakrilat (EDGMA)'nın miniemülsiyon polimerizasyon reaksiyonuyla nanopartiküller hazırlanmıştır.

Nanopartiküller zeta-boyut ölçümleri ile karakterize edilmiştir. Polimeri QCM çipine uygulamadan önce yüzey daha da değiştirildi ve etkinleştirildi. Başlangıçta, QCM çipinin yüzey modifikasyonu 11-merkaptodekanoik asit (MUA) kullanılarak gerçekleştirilmiştir ve polimere bağlanacak şekilde aktive edilmesi için karbodiimid olarak bilinen EDC/NHS etil-3-(3-dimetilaminopropil) / N-hidroksisüksinimid kullanılmıştır. Poli (2-hidroksietil metakrilat) nanopartikülleri P(HEMA-NPs), MUA'da mevcut karboksil grubunu bağlamak üzere polimerin hidroksil grubunu bir nitrojen grubuyla değiştirmek amacıyla 3-aminopropiltrietoksi silan (APTES) ile etkinleştirilmiştir. Çip hazırlama ve polimer modifikasyonu sonrasında, MM hücre yüzeylerinde yaygın olan CD44'e özgü DF6392 antikorları yüzeye bağlanması etkinleştirilmiştir. Nanopartikül kaplı ve antikora bağlı QCM çiplerine atomik kuvvet mikroskobu (AFM), fourier dönüşümü kızılötesi zayıflatılmış toplam yansıma (FTIR-ATR) spektroskopi ve temas açısı ölçümleri yoluyla karakterize edilmiştir.

A375 hücre örnekleri, karakterizasyon çalışmalarının ardından, fonksiyonelleştirilmiş QCM çipine 1 mL/dk akış hızında eklenmiş ve rezonans frekansı (f) kaydedilerek kinetik, afinite çalışmaları ve adsorpsiyon modelini belirlemek için sayıları 50 ila 5000 hücre/mL arasında değişen çeşitli konsantrasyonlarda kullanılmıştır. Bağlama modu Langmuir izoterm modeline uygun olduğu tespit edilmiştir. DF6392 antikorları ile işlevselleştirilmiş QCM çipinin seçiciliğini göstermek için, insan pankreas kanseri hücre dizisi PANC-1 ve insan embriyonik böbrek 293 hücre HEK293, 2500 hücre/mL oranında çip üzerinde rekabetçi bir şekilde adsorbe edilip hücre/cm^2 birim yüzeyindeki kütle değişiklikleri (Δm) sensör gerçek zamanlı olarak tespit edilmiştir. Sistemin tespit limiti 1.2 hücre/mL dir. QCM biyosensörü, A375 hücreleri için PANC-1 hücrelerine göre 23.34 kat ve HEK293 hücrelerine göre 9.24 kat daha seçici çıkmıştır. Antikor ile işlevselleştirilmiş sistem, MM hücrelerinin etkili bir şekilde tespit edilmesi konusunda ümit vericidir. Bu bulgular, QCM biyosensörünün kanser hücresi tespiti için uygun, oldukça seçici, verimli ve hassas bir sistem olduğunu göstermektedir.

Anahtar Kelimeler: QCM Biyosensör, CD44 Reseptörleri, Malign Melanom, DF6392 antikorları, P(HEMA-NPs).

ABSTRACT

DESIGN AND OPTIMIZATION OF QCM BIOSENSOR TO DETECT MALIGNANT MELANOMA CELLS VIA THEIR CD44 RECEPTORS

Rahaf Sameer Taofek AIOSH

Master of Science, Department of Chemistry

Supervisor: Assoc. Prof. Dr. Erdoğan ÖZGÜR

June 2024, 86 pages

Malignant melanoma (MM) is a highly aggressive form of skin cancer originating from melanocytes, presents a significant public health concern globally. Its rising incidence and propensity for metastasis underscore the critical need for innovative diagnostic approaches to enable early detection and intervention. In this study, we address this pressing issue by proposing the design and optimization of a quartz crystal equilibrium (QCM) biosensor capable of detecting MM cells through CD44 (cluster of differentiation 44) receptors. Which is very highly expressed on the surfaces of MM cells. We aimed to identify these cells by combining QCM with the CD44-binding antibody DF6392. In the first step, to enhance the QCM chip's surface area, nanoparticles were synthesized through a miniemulsion polymerization process involving (EDGMA) ethylene glycoldimethacrylate and (HEMA) 2-hydroxyethyl methacrylate. The nanoparticles underwent characterization using zeta-sizer measurements. Prior to applying the polymer

onto the QCM chip, additional modification and activation of the surface were carried out. Initially, QCM chip underwent surface modification with 11-mercaptoundecanoic acid (MUA) to enable polymer binding. N-hydroxysuccinimide (NHS) and ethyl-3-(3-dimethylaminopropyl) carbodiimide (EDC) were employed for activation purposes. The functionalization of poly(2-hydroxyethyl methacrylate) nanoparticles (P(HEMA-NPs)) was conducted using (APTES) (3-aminopropyltriethoxy silane) in order to replace the polymer's hydroxyl group with a nitrogen group to bind to the existing carboxyl group in MUA. After chip preparation and polymer placement, we modified DF6392 antibodies specific to (CD44), prevalent on (MM) cell surfaces. The QCM chip underwent immobilization of antibodies. Following this, the QCM chip coated with nanoparticles and attached with antibodies underwent characterization using (AFM) (atomic force microscopy), (FTIR-ATR) Spectroscopy (Fourier transform infrared-attenuated total reflectance), and contact angle measurements. After the characterization studies, the functionalized QCM chip was exposed to A375 cell samples spanning from 50 to 5000 cells/mL at a flow rate of 1mL/min, and (f) (the resonance frequency) was then recorded, to carry out kinetic, affinity studies and to determine the adsorption model. The Langmuir isotherm model provides the best fit for the binding mode. To demonstrate the selectivity of the modified QCM chip with DF6392 antibodies, (HEK293) human embryonic kidney 293 cell line, and (PANC-1) human pancreatic cancer cell line, were absorbed onto the QCM chip in competition, at a rate of 2500 cells/mL. Real-time detection was employed to monitor the mass changes (Δm) on the sensor's surface, measured in cell/cm^2 units. (LOD)(the system's detection limit) stood at 1.2 cells/mL. The QCM biosensor exhibited 23.34 times greater selectivity for A375 cells compared to PANC-1 cells and 9.24 times more selective than HEK293 cells. This receptor antibody-functionalized system shows promise for effectively detecting MM cells. These findings indicate that the QCM biosensor is a highly selective, efficient, and sensitive system suitable for cancer cell detection.

Keywords: QCM Biosensor, CD44 Receptors, Malignant Melanoma, DF6392 Antibodies, P(HEMA-NPs).

ACKNOWLEDGEMENTS

All glory and gratitude belong to the Almighty Allah, who has been my steadfast source of strength, and to whom I attribute all that I have achieved and accomplished.

I extend my deepest gratitude and heartfelt appreciation to all those who have supported me throughout this study. Special acknowledgment is reserved for my supervisor, Assoc. Prof. Dr. Erdoğan ÖZGÜR, for their invaluable guidance and assistance. The steadfast support he provided, patience, generous comments, and invaluable advice were indispensable in completing this work. I am truly grateful that he reached out to me with great understanding and patience, extending a helping hand that made a significant difference throughout my educational pursuit. I would like to express my sincere thanks to Prof. Dr. Adil Denizli and Prof. Dr. Handan Yavuz for their exceptional support, both scientifically and morally, during the course of my master's thesis. Their guidance in research has been instrumental, and the profound care and affection they have shown me have been a source of inspiration. I am indebted to them for their unwavering encouragement and for the invaluable contribution they have made to my academic journey. Special thanks to Prof. Dr. Ayşe Kevser Özden for her invaluable support and provision of essential cells and materials, which significantly contributed to the success of my master's research. Your generosity and support have truly propelled my work forward, and I am deeply thankful for your kindness and guidance. I extend my heartfelt thanks to all members of the Bioreg family for their invaluable assistance and kind sentiments. Your support has been truly appreciated, and I am grateful for the feeling of friendship you have given me. I'm also thankful to the examination committee members, for their valuable and fruitful discussions.

My family deserves all my gratitude and affection, who were Rahaf's first supporters and believed in me and my dreams. They have been instrumental in helping me reach this moment. Additionally, heartfelt thanks to my companion on this journey, my childhood friend and my hero who stood by my side at every step with unwavering support and love. To my family and my dear hero, I love you very much, and I am committed to doing my best to always be a source of pride for you.

RAHAF SAMEER TAOFEK AIOSH

TABLE OF CONTENTS

INDEX OF FIGURES

INDEX OF TABLES

SYMBOLS AND ABBREVIATIONS

SYMBOLS

f_0	Resonance Frequency of The Fundamental Mode
μ_q	Shear Modulus
ρ_q	Density of Quartz (ρ = 2.648 g/cm^3)
Δm	Surface Mass Loading
A	Piezoelectrically Active Gold Disk Area
$\Delta m/A$	The Mass İncrease Per Unit of Area (ng cm^{-2}).
F	The Resonance Frequency
rpm	Revolutions Per Minute
mg	Milligram
mL	Milliliter
Mw	Molecular Weight
pH	Power of Hydrogen
mM	Millimole Per Liter
µL	Microliter 1 × 10^{-6} liters
h	Hour
min	Minute
°C	Celsius
kHz	Kilohertz
µm/s	Micrometers Per Second
MHz	Megahertz

ABBREVIATIONS

MM	Malignant Melanoma
UV	Ultraviolet Radiation
QCM	Quartz Crystal Microbalance
CD44	Cluster of Differentiation 44
P(HEMA-NPs)	Poly(2-Hydroxyethyl Methacrylate) Nanoparticles
IARC	International Agency For Research On Cancer
BCC	Basal Cell Carcinoma
SCC	Squamous Cell Carcinoma
SSM	Superficial Spreading Melanoma
NM	Nodular Melanoma
LMM	Lentigo Malignant Melanoma
RGP	Radial Growth Phase
VGP	Vertical Growth Phase
EMT	Epithelial-To-Mesenchymal Transition
AJCC	American Joint Committee on Cancer
IARC	International Agency for Research on Cancer
NCCN	National Comprehensive Cancer Network
ASCO	American Society of Clinical Oncology
SLNB	Sentinel Lymph Node Biopsy
CT	Computed Tomography
MRI	Magnetic Resonance Imaging
ECM	Extracellular Matrix
SPR	Surface Plasmon Resonance
WHO	World Health Organization's
AT	Analog Transverse
BT	Blank Transverse
AC	Alternating Current
AFM	Atomic Force Microscopy
FTIR-ATR	Fourier Transform Infrared-Attenuated Total Reflectance
Ab-NPs QCM	Antibody-Nanoparticles Quartz Crystal Microbalance
DNA	Deoxyribonucleic Acid
CCND1	Cyclin D1 Gene

HA	Hyaluronic Acid
EDGMA	Ethylene Glycol Dimethacrylate
HEMA	Hydroxyethyl Methacrylate
SEM	Scanning Electron Microscopy.
SDS	Sodium Dodecyl Sulfate
APS	Ammonium Persulfate
PVA	Polyvinyl Alcohol
$NaHCO_3$	Sodium Bicarbonate
$NaHSO_3$	Sodium Bisulfite
EDC	Ethyl-3-(3-Dimethylaminopropyl) Carbodiimide
NHS	N-hydroxysuccinimide
MUA	11-Mercaptoundecanoic Acid
APTES	3-Aminopropyltriethoxy Silane
PBS	Phosphate Buffered Saline
H_2SO_4	Sulphuric Acid
H_2O_2	Hydrogen Peroxide

1. INTRODUCTION

Cancer disrupts the normal balance of homeostatic control due to the gathering of epigenetic and genetic irregularities results in uncontrolled cell growth [1]. Each year, MM accounts for 55500 deaths, along with mortality and incidence rates varying globally based on access to early detection. Despite limited treatment options for over 40 years, recent advancements in biological understanding and therapeutic substances have transformed advanced MM treatment. The process of melanocytes turning malignant and leading to metastatic (MM) is a complex interplay of external and internal triggers, along with factors intrinsic to the tumor and those related to the immune system. While melanocytes typically undergo rare divisions, occurring fewer than twice a year, the rate of cell proliferation steadily increases as melanocytic neoplasms advance sequentially [2, 3]. Commonly recognized risk factors comprise ultraviolet (UV) radiation, specific types of moles, indoor tanning, a history of melanoma either in oneself or in the family, and specific phenotypic characteristics [4, 5].

MM severity is primarily determined by tumor thickness, categorized as either localized or spread beyond visible areas. Spreading deep into the skin enables MM cancer cells to enter small lymph vessels, providing a pathway for potential spread to distant parts of the body [6].

UV has been demonstrated to generate DNA damage through photosensitive reactions, leading to the formation of reactive oxygen species. These species have the potential to cause chromosomal abnormalities, mutations, single-strand breaks, and sister chromatid exchanges , ultimately leading to cell damage and the development of cancer [7]. Early and accurate detection is crucial to halt the advancement of a disease and disrupt the transmission chain and biosensors offer a rapid, cost-effective alternative to traditional assays. Biosensors serve as analytic tools designed to detect biomolecules. They find applications in clinical settings, specifically for identifying disease-related markers in biological fluids [8, 9], and piezoelectric biosensor, like Quartz Crystal Microbalance (QCM), provide high sensitivity, real-time monitoring, detection without the need for labels, portability, stability, and seamless integration with contemporary technologies

[10]. QCM biosensor systems consist of a slender piece of AT-cut quartz crystal placed between dual electrodes. These devices, sensitive to nanograms are capable of detecting changes in the (f) of the quartz crystal when (m) is added or removed from the surface under the influence of potential energy [11].

Cancer cell membrane changes, particularly the Cluster of Differentiation 44 (CD44) receptors, serve as targets for detection. In the process of cancer metastasis, CD44, a family of adhesion molecules, assumes a pivotal role. The expression level of CD44 is particularly significant in cancer metastasis, with higher expression observed on the metastatic MM surface compared to their less metastatic counterparts. Monitoring changes in CD44 levels on the surface of MM functions like a specific and sensitive marker for cancer [12]. The piezoelectric immunosensors' potential, featuring specific receptor-ligand interactions, is experiencing rapid expansion because of their high specificity and sensitivity towards cancer cells. Our aim has been to design and optimize the QCM biosensor for detecting MM cells via their CD44 receptors. This is done by modifying the QCM biosensor's surface and linking it with P(HEMA-NPs) to increase the surface area and linking it with DF6392 antibody, which specifically binds to CD44 receptors. The primary objective behind the development of this QCM biosensor for MM cancer cells involves proving the efficacy of systems designed to pinpoint alterations in the cell membrane and aims to showcase the sensor's ability to accurately detect these cells, particularly those circulating in the bloodstream, using a swift and cost-effective method. When passing a sample containing MM cells, CD44 receptors binds to DF6392 antibody, and their binding leads to an increase in (m) on the QCM surface, led to a alteration in the (f) value, which can be calculated and detect the presence or absence of CD44 receptors.

2. GENERAL INFORMATION

2.1. Skin Cancer

Skin cancer develops when genetic mutations cause uncontrolled growth of skin cells. This condition is scientifically defined by the abnormal and uncontrollable division of skin cells, a process often triggered through exposure to (UV) from artificial sources (tanning beds) and sunlight. The UV radiation possesses the capability to damage the DNA within skin cells, resulting in genetic mutations that disrupt normal cell regulation mechanisms. Over time, the accumulation of these genetic abnormalities may culminate in the formation of cancerous lesions on the skin. Skin cancer represents a significant public health concern due to its increasing incidence. Approximately 1.5 million new cases of skin cancer were reported according to The (IARC) International Agency for Research on Cancer in 2020. The greatest danger in skin cancer is the possibility of metastasis, as the cancer can spread to vital organs and become difficult to treat. It can infiltrate the surrounding tissues and pose a greater risk of complications. Understanding the underlying cellular and molecular changes that lead to skin cancer is crucial for its prevention and management. Early detection through regular skin examinations is also crucial for improving outcomes, as treatment tends to yield higher success rates when skin cancer is detected during its early stages [13-15].

2.1.1. Types of Skin Cancer

Skin cancer is categorized based on its histological origins. The three primary histological types include (MM) malignant melanoma, (BCC) basal cell carcinoma, and (SCC) squamous cell carcinoma. BCC is the most common form. This malignancy originates from basal cells situated near the epidermis-dermis junction. BCCs typically appear like pinkish patches, pearl-like bumps, or flesh-colored rounded growths on the skin.

(SCC) holds the position as the second most frequently occurring form, originating from flat and thin squamous cells located in the (epidermis). SCCs usually present as red, firm bumps, scaly patches, or sores that may undergo cycles of healing and reopening.

(MM), is referred to as the most dangerous type owing to of its rapid metastasis to distant organs throughout the body. MM cancer originates from melanocytes, specialized pigment-producing cells. It may arise either from pre-existing moles on the skin or present as newly formed dark spot that stands out from the surrounding skin [16, 17].

2.2. Malignant Melanoma (MM) Cancer

Skin cancer is on the rise globally, with a significant surge in both cases and fatalities. MM stands out as the primary cause of mortality among malignant skin cancers, recognized for its aggressive behavior. Globally, the incidence of melanoma (MM) cancer is increasing, prompting a heightened focus on this area in cancer research. According to a recent study, although (MM) represents just 4% of all skin cancer cases, it accounts for a staggering 75% of deaths related to skin cancer. Notably, this percentage has seen a more rapid increase over the past 50 years compared to almost any other cancer type [18]. Men exhibit a higher incidence of (MM) compared to women. Furthermore, its incidence rises with age, with the highest number of new cases occurring in the 65–74 age group [13-16, 18, 19].

MM cancer, originates from melanocytes, which can be located in the skin, mucous membranes, or pre-existing moles. It primarily manifests in areas of the skin exposed to sunlight, including the chest, neck, back, and legs. However, there are instances of occurrence in non-sun-exposed areas and even within the eyes. The development of MM cancer is influenced by various factors, encompassing genetic and environmental components. These factors encompass the presence of numerous moles or, a family history of MM cancer, skin type, and environmental factors like UV, which can lead to genetic mutations. MM cancer, when detected late and characterized by increased tumor thickness, poses significant challenges for removal and successful treatment. Therefore, early detection of malignant melanoma plays a pivotal role in enhancing survival rates [18-21].

2.2.1. Classification for MM Cancer

There is a histological classification system for MM cancer developed by Dr. Wallace Clark that classifies it into distinct subtypes based on the histopathological characteristics of the cancer cells within the layers of the skin, especially within the epidermis and dermis. This classification has contributed to the understanding of the development, diagnosis and treatment of MM cancer [17].

Some common histological subtypes include:

1. (SSM) Superficial Spreading Melanoma: This subtype holds the distinction of being the most prevalent. It appears as irregularly shaped moles with various colors. In this subtype, MM cancer cells initially spread on the surface of the skin before invading the deeper layers.
2. (NM) Nodular Melanoma: This subtype grows rapidly and often presents as a raised bump with colors like black, blue, or red. It tends to penetrate deeper into the skin without the typical gradual growth phase seen in other subtypes.
3. (LMM) Lentigo Malignant Melanoma: Typically, this subtype impacts skin areas consistently exposed to sunlight, such as the forearm or neck and head region. LMM appears as a large, flat patch with tan or brown color and uneven edges. It is characterized by irregularly shaped MM cancer cells along the junction of the epidermis of the skin and the dermis.

After this classification, other types were identified, for example: naevoid melanoma, desmoplastic melanoma, mucosal melanoma, and acral lentiginous melanoma. However, the World Health Organization still adopts the Clark classification, including SSM, LMM, and NM.

2.2.2. Stages of MM Cancer

Cancer staging is vital, encompassing the assessment of cancer's spread and its specific location within the body. Doctors utilize the assessment of the primary tumor's size and the determination of cancer spread to develop a prognosis and tailor a personalized treatment plan for each patient. The development of MM cancer can be divided into two main stages. MM commonly entails mutations that result in the loss of function in cell cycle regulator genes and tumor suppressor genes, such as the Cyclin D1 gene (CCND1), which contribute to the continued progression of the disease. The severity of the cancer depends mainly on the thickness of the tumor. Scientist Wallace Clark developed a model to classify the stages of MM cancer growth, which are as follows: Radial Growth Phase (RGP): This is the first stage in which the cancer cells have not spread beyond the area surrounding the abnormal skin growth. At this stage, a surgical procedure, known as a lumpectomy, is performed in which the tumor and a portion of nearby healthy skin with defined oval borders are removed and is usually effective. During the Vertical Growth Phase (VGP), which is the second stage, MM cells start infiltrating the deeper layers of

the skin by crossing the basement membrane. In this stage, cancer cells have the ability to spread to distant areas of the body through the bloodstream and lymphatic vessels, resulting in metastatic or advanced-stage skin cancer. Measuring the thickness of MM cancer, known as the Breslow Score, enables doctors to assess the transition from RGP to VGP. This is essential because a slight difference in millimeters distinguishes between treatable, early-stage MM and an aggressive, incurable cancer. One way cancer cells spread in the body is through the (EMT) process Epithelial-To-Mesenchymal Transition. This makes MM cells less sticky and changes their shape to make them better at moving around, invading other areas, and forming new growths in different parts of the body, which are called metastases [22].

The (AJCC) "American Joint Committee on Cancer" has devised a novel staging system for MM cancer. Based on the eighth edition, which was released on 1 January 2018 [23]. The stages are determined based on tumor thickness (T), lymph node involvement (N), and distant metastasis (M).

2.2.3. Incidence and Mortality Rates of MM Cancer

According to the (IARC) skin cancers, including MM, in 2020, an estimated 1.5 million new cases of melanoma were diagnosed worldwide, making it one of the most frequently diagnosed cancers globally. Specifically, in the same year, approximately 325000 cases were diagnosed globally, which resulted in 57000 deaths. New Zealand and Australia exhibited the highest incidence rates, trailed by Northern Europe, Northern America, and Western Europe. Conversely, most countries in Asia and Africa reported very low incidence rates. MM cancer can impact individuals of all skin types, despite those with fairer skin being at a greater risk. Unfortunately, MM cancer tends to be diagnosed at a more advanced stage in individuals with darker skin types, resulting in a poorer prognosis [24].

A recent study, published in the journal JAMA Dermatology, conducted by scientists from the IARC and their collaborators predicts anticipate a substantial rise in the number of new MM cases in the coming two decades. It delivers a detailed examination of the global burden of MM in the year 2020, as well as projections for the numbers for new cases and fatalities up to the year 2040. New cases are projected to surge by more than 50%, surpassing 500000 cases annually. Additionally, fatalities are expected to rise by more than two-thirds, reaching nearly 100000 deaths annually [24].

2.2.4. Treatment of MM Cancer

Chemotherapy has limited effectiveness in the treatment of MM cancer. However, there has been a reduction in mortality rates of approximately 4% in recent years, thanks to advancements in targeted therapies and immunotherapies for the disease [19].

There are many treatment options that are determined based on factors such as the distinctive features of the tumor, the disease stage, and individual patient factors. Some treatment options recommended according to (NCCN) and (ASCO) include:

- Surgical Excision: Treating early-stage MM typically involves surgically removing the tumor alongside a margin of healthy tissue, with the extent of the procedure determined by the tumor's thickness and depth. The aim is complete cancer removal and lowering the chance of it coming back [20, 25].

- Adjuvant Therapy: Adjuvant therapy refers to treatments given after surgery to lower the likelihood of cancer. In MM, adjuvant treatment options encompass targeted therapy and immunotherapy. Therapy selection is contingent upon the individual's traits and the stage of melanoma [26].
- Immunotherapy: Immunotherapy drugs, such as immune checkpoint inhibitors, are used to enhance the immune system's response against MM. Drugs like pembrolizumab and nivolumab work by blocking proteins that inhibit immune system activity, allowing immune cells to recognize and attack cancer cells [27].
- Radiation therapy: High-energy radiation is employed to eliminate cancer cells or reduce tumor size. It can serve as supplemental therapy following surgery or for symptom relief in advanced cases [28].
- Chemotherapy: While less common in MM treatment, chemotherapy drugs may still be used in specific cases, particularly when MM has spread to distant organs [25].

2.2.5. The Importance of Early Detection of MM Cancer

When MM cancer is diagnosed early, it is typically limited to the skin and can often be cured through surgical removal. In contrast, advanced MM cancer that has spread (metastatic melanoma) require more intense therapies like targeted treatments, immunotherapy, or chemotherapy. Early detection and treatment are linked to better survival rates. Localized MM has a significantly higher five-year survival rate compared to metastatic MM. Early detection allows for timely intervention, preventing its progression. By identifying MM at an early stage, it can be removed before it penetrates deeper layers of the skin or spreads to other organs. This reduces the risk of metastasis and minimizes the need for more aggressive and potentially less effective treatment options. Early-stage MM tend to be smaller and localized, which means surgical removal can be less extensive. Smaller procedures lead to shorter recovery times, lower complication risks, and better cosmetic results. Early detection may spare patients from more extensive surgeries or the need for reconstructive procedures. Early detection brings peace of mind and reduces anxiety for individuals at risk of MM or with suspicious skin lesions. Timely diagnosis and treatment alleviate uncertainty and stress associated with a

potential cancer diagnosis, empowering individuals to take proactive steps in managing their health and well-being [25, 29, 30].

2.2.6. Current Diagnostic Methods and Their Limitations

There are different diagnostic methods that are frequently used to detect MM cancer. Some of these methods include:

- Clinical Evaluation: Dermatologists or healthcare providers thoroughly examine the skin, assessing suspicious lesions or moles. They consider various factors such as size, shape, color, and border irregularities, to determine if further evaluation is necessary. However, this method cannot conclusively confirm the diagnosis and is vulnerable to possible misdiagnosis or delayed diagnosis [31, 32].
- Dermoscopy: This non-invasive technique involves using a dermatoscope, a specialized tool that provides magnified views of skin lesions. Dermoscopy helps identify specific features associated with MM cancer and aids in making accurate diagnoses. However, this examination is still subjective and relies on the expertise of the dermatologist [31, 32].
- Biopsy: If a lesion is suspected to be MM cancer based on clinical evaluation and dermoscopy, a biopsy is performed to obtain a tissue sample for further examination. Different types of biopsies can be conducted, including punch, incisional, or excisional biopsy. Following, the sample is forwarded to a pathology laboratory. Here, a pathologist scrutinizes it under a microscope to verify the existence of MM and evaluate its distinct characteristics, like the presence of ulceration, type, and thickness. However, there are certain limitations associated with this procedure. Sampling error can occur, where the biopsy may not capture the most aggressive or representative areas of the tumor, leading to an incomplete or inaccurate diagnosis. Additionally, since a biopsy is an invasive procedure, there are inherent risks such as bleeding, infection, or scarring. There is also a possibility of false-negative results, especially if the biopsy samples are inadequate or if the MM cancer is in its early stages [33, 34].
- (SLNB) Sentinel Lymph Node Biopsy: When there's a potential for MM cancer to spread to nearby lymph nodes, (SLNB) might be advised in specific cases. The first lymph node to be impacted by the spread of cancer is called

the sentinel lymph node. This procedure involves injecting a radioactive substance or dye near the tumor to identify this node. Following that, they undergo surgical removal and examination to detect cancer cells, aiding in determining the extent of disease involvement [22].

- Imaging Tests: Depending on the stage and characteristics of the MM, additional tests involving imaging techniques such as (MRI) Resonance Imaging, or (CT) Computed Tomography, may be conducted. Such imaging tests aid in assessing the disease's scope and detecting potential metastasis to other body areas. These steps are crucial for accurately diagnosing MM and determining appropriate treatment strategies based on the stage and characteristics of the disease. However, these imaging tests have limitations in detecting small or early-stage lesions. They are typically more valuable for evaluating advanced MM cancer and potential risk of additional radiation exposure [35, 36].

Overall, it's noticeable that several current methods lack one or more of the essential qualities: simplicity, selectivity, sensitivity, and speed. These are important factors to consider when evaluating the effectiveness and practicality of existing techniques.

2.2.7. The Need for More Sensitive and Specific Detection Methods

Although current diagnostic methods such as clinical evaluation, dermoscopy, and biopsy have value, they have limitations as mentioned previously so there is a distinct necessity to advance methods that are more specific and sensitive in detecting MM cancer. More sensitive methods can identify MM at its earliest stages when it is most manageable and curable. Current diagnostic methods may occasionally miss or misdiagnose MM, leading to false-negative results. More sensitive methods can help minimize false negatives, improving diagnostic accuracy and ensuring appropriate treatment [13, 31, 37].

Many benign skin lesions, such as moles or non-cancerous tumors, can resemble MM cancer, posing diagnostic challenges. More specific detection methods capable of accurately distinguishing MM from benign lesions would help enhance patient privacy and reduce unnecessary biopsies and surgeries for benign lesions, reducing patient anxiety, discomfort, and healthcare costs [31, 34].

Some MM cancer exhibit atypical features or arise in challenging locations, making them difficult to diagnose accurately. More sensitive and specific methods can aid in detecting these lesions and guiding appropriate management decisions [31]. In this study, we chose

the QCM biosensor as a sensitive, fast, and highly accurate detection tool for detecting CD44 associated with MM.

2.3. CD44 Receptors

2.3.1. Definition and Characteristics of CD44 Receptors

The molecular structure of cancer cell membranes can undergo changes that can be targeted for therapeutic or diagnostic purposes. One specific target is the CD44 receptors, which is part of a family of adhesion molecules (CD44 receptors enables cells to adhere to their surroundings and form stable structures) and participates in numerous biological functions including migration, proliferation, and cell division. The gene responsible for encoding the CD44 receptor, which is a transmembrane glycoprotein, is situated on chromosome 11 in humans. Monitoring changes in CD44 levels serve as a specific and sensitive marker for detecting cancer. Molecular methods, including the detection of CD44 expression, are used to detect biomarkers in MM cells. The expression level of CD44 has a critical role in the metastasis of cancer as CD44 is found in both benign and MM cancer, but its expression is more pronounced in MM tumors. Alterations in the expression pattern of these molecules can have two effects. Firstly, they can disrupt normal cell interactions, leading to structural and functional disorganization. Secondly, they have the potential to stimulate both migration and cell proliferation. These characteristics are commonly observed in cancer cells, indicating the potential role for these molecular changes in the development and progression of cancer [12, 38, 39].

2.3.2. CD44 Receptors Structure and Function

CD44 acts as the primary receptor for (HA) Hyaluronic Acid on the surface of the cell. It is a glycoprotein that comprises three components: an extracellular, a transmembrane, and an intracellular. CD44 also acts as a signaling receptor, conveying signals from outside the cell into its interior and influencing critical cellular processes such as survival, proliferation, differentiation, and cytoskeletal rearrangements. CD44 exists in various isoforms as a result of post-translational modifications and alternative splicing. The main isoform is CD44s, which is involved in basic cell functions. CD44 also has variant CD44v isoforms, including CD44v6, characterized by additional exons, and they contribute to processes such as cancer progression and metastasis. The isoforms contribute to the versatility of CD44, impacting cell adhesion, migration, and signaling in different ways,

making CD44 a significant player in various cellular functions and disease processes [12, 38, 40].

As shown in the Figure 2.1, the structure of the CD44 receptor consists of:

- Extracellular Domain: Extends outside the cell membrane and includes linker regions (L) that vary in number depending on the isoform. It contains a hyaluronic acid binding domain for interaction with hyaluronic acid and other extracellular matrix components.
- Transmembrane Domain: Extends across the cell membrane, providing stability to the glycoprotein within the lipid bilayer. This domain is composed of hydrophobic amino acids that facilitate its integration into the membrane structure.
- Cytoplasmic Domain: Located on the intracellular side of the cell membrane. This intracellular region interacts with signaling molecules, proteins, and the cytoskeleton, facilitating signal transduction and intracellular processes.

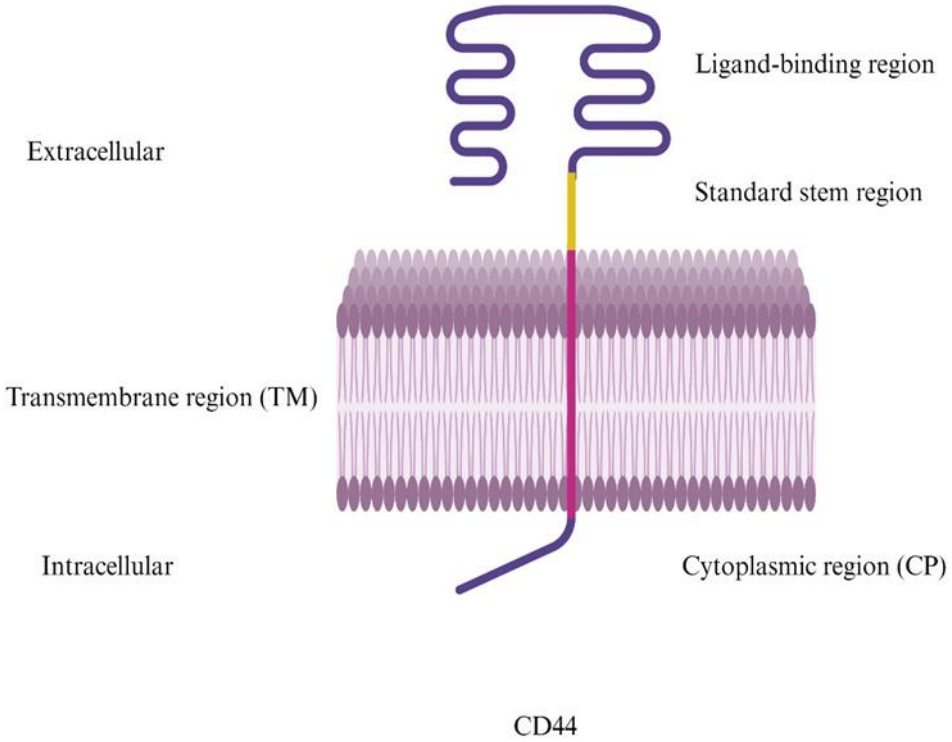

Figure 2.1. Structure of the CD44 receptor. This illustration, obtained from [38], has been edited for clarity.

2.3.3. Role of CD44 Receptors in MM Cancer Progression and Metastasis

Immunohistochemistry analysis for MM tumor in different stages showed an elevated expression of CD44. In MM cancer cells, CD44 is involved in abnormal processes like revascularization and inflammation, as well as the multiplication and adhesion of cells. CD44 promotes the invasion of MM cells by facilitating interactions with components of the Extracellular Matrix (ECM), such as HA and other adhesive molecules. This enables MM to metastasize to surrounding tissues by detaching from the primary tumor. It enables MM cells to survive in the bloodstream, adhere to the inner lining of blood vessels at distant sites, and extravasate into surrounding tissues, forming secondary tumors. CD44 mediated signaling pathways and interactions with the ECM may confer a survival advantage to MM cells, allowing them to evade the effects of therapeutic interventions [41-44].

2.3.4. CD44-Detection Using Biosensor

Cancer is prevalent, yet recent improvements have been noted in survival rates. Nevertheless, due to the limitations of cancer analysis techniques, the actual survival rate of patients remains uncertain. This underscores the importance of early-stage cancer diagnosis for effective detection. Using biomarkers like CD44, which is linked to MM cancer, can help overcome these challenges. By focusing on these markers, we might enhance how we detect and treat cancer more accurately and quickly. Now biosensors are used to detect CD44, such as electrochemical biosensors. These biosensors use changes in electrical properties to detect the presence of CD44. Electrode surfaces are modified with CD44-specific antibodies. When CD44 molecules bind to the surface, it leads to a change in the electrochemical signal. Measuring this signal correlates directly with the concentration of CD44 in the sample [44, 45].

There are also (SPR) surface plasmon resonance biosensors, which are optical biosensors whose working principle is based on tracking differences in the refractive index on the surface of the chip. This surface is equipped with CD44-specific capture molecules that lock it into place. When CD44 binds to this surface, it induces a shift in the SPR signal, allowing real-time measurement. This method offers insights into the presence and binding kinetics of CD44 within the sample. Detection using biosensors offers numerous advantages, including sensitivity, specificity, and real-time or rapid detection capabilities [45, 46]. There are other types of biosensors that have been used, but there is no study that has used QCM to detect CD44 as a biomarker for MM.

2.4. Biosensors

2.4.1. Definition and Principles of Biosensors

Biosensors, utilized in biotechnology fields, food safety, healthcare, and environmental monitoring, are excellent analytical tools for detecting the biological analyte, whether its presence or concentration. They play crucial roles in environmental analysis, drug discovery, disease diagnosis, and quality control. They combine biological recognition element with transducer to analyze specific substances (analytes) in a sample. This recognition element can be various biological components like enzymes, antibodies, or nucleic acids, depending on what needs to be detected. Biosensors offer fast, sensitive, and selective analyte detection, making them valuable for research and practical use. They

demonstrate high performance and gives repeatable results. They are easy to use, provide real-time monitoring, and label-free. Systems that don't require labeling, such as this one, offer convenience by lowering costs, cutting down on sample preparation time, and allow direct monitoring of ongoing reactions. Within a biosensor, the essential components include the recognition element (receptor), which engages with the analyte, and the signal transducer, responsible for converting the recognition event into a signal that can be detected. This interaction causes a noticeable change in the sensor system. Then, there's the transducer, which converts this interaction into a measurable signal. For meaningful measurements, biosensors need calibration. This means establishing a connection between the measured signal and the concentration or activity of the target analyte. Scientists use calibration curves or standard reference materials for this. Once calibrated, the biosensor can output a signal that is analyzed to figure out if and how much of the target analyte is present. This analysis might involve techniques like signal processing, algorithms, or comparing with known standards [8, 27, 47, 48].

2.4.2. Types of Biosensors

Varied types of biosensors include mass-based, optical, piezoelectric, thermal, magnetic, and electrochemical biosensors, offer a spectrum of options for tailored applications, making them indispensable tools in the realm of modern sensing technologies. Each type has its advantages and limitations, and the choice of the suitable biosensor relies on the particular application needs, analyte traits, and preferred detection parameters.

1- Electrochemical biosensors harness the electrochemical characteristics of the interaction between the recognition element and the analyte to produce an electrical signal. Their functionality relies on principles such as amperometry and potentiometry, like the Amperometric biosensor. 2- Optical biosensors identify alterations in light properties arising from the recognition event. These biosensors utilize techniques like absorbance or Surface Plasmon Resonance (SPR) to gauge the interaction between the recognition element and the analyte. 3- Piezoelectric biosensors measure changes in mass during the recognition event. These sensors typically use a piezoelectric crystal, such as quartz, which generates a change in resonance frequency like Quartz Crystal Microbalance (QCM) [27, 49, 50].

2.4.3. Applications of Biosensors in Medical Diagnosis

Present methods for identifying both non-infectious and infectious diseases are largely laborious, costly, and fail to meet the standards outlined by the (WHO). These standards encompass affordability, sensitivity, specificity, user-friendliness, speed, robustness, absence of equipment dependency, and ease of delivery to end-users. Consequently, there is a demand for biosensors that fulfill these WHO criteria.

In medical diagnosis, biosensors play a vital role, revolutionizing disease detection, monitoring, and patient care with their wide-ranging applications. Biosensors play a pivotal role in various aspects of healthcare. For individuals with diabetes, biosensors provide a convenient and rapid way to monitor blood glucose levels. In infectious disease detection, biosensors enable swift and sensitive identification of infectious agents like bacteria, viruses, and parasites by pinpointing specific biomarkers associated with infections. Genetic testing benefits from biosensors as they can detect specific DNA sequences or mutations linked to inherited disorders, supporting applications in prenatal screening and personalized medicine. Biosensors also contribute to optimizing drug dosages in the body, ensuring efficacy while minimizing side effects. Furthermore, they swiftly identify allergens, aiding in allergy diagnosis and management by detecting specific proteins or antibodies in biological samples. In cancer diagnosis, biosensors are instrumental in detecting specific biomarkers, facilitating early detection, targeted therapies, and ongoing treatment monitoring [51, 52].

2.4.4. Advantages of Biosensors for Cancer Detection

Biosensors stand out for being rapid, offering real-time results, and portability. Due to their distinctive features, biosensors hold significant potential in cancer detection. With their high sensitivity and low detection limit, biosensors prove highly effective for diagnosing different types of cancer. Traditional diagnostic techniques require a billion cells in tumor tissue, which typically range in diameter 7-10 nm. It is worth noting that biosensors can detect cancer even in a few million malignant cells, which is a unique advantage. This enhanced sensitivity positions biosensors as promising tools for early and precise cancer detection. This specificity helps minimize false-positive results and enhances the accuracy of cancer diagnosis. This is particularly crucial in cancer cases, where early detection can significantly improve treatment outcomes. Biosensors offer the advantage of utilizing non-invasive sample types like blood, saliva, or urine for cancer

detection. This approach makes the testing process less invasive and more patient-friendly when compared to traditional biopsy methods [41, 42].

Biosensors hold the potential for being designed as portable, point-of-care devices, usable directly at the patient's location, whether at clinics or even at home. This accessibility enhances the feasibility of early and convenient cancer screening, particularly in areas with limited resources. In addition, it can be designed to detect multiple cancer biomarkers simultaneously, enabling the detection of different types or stages of cancer in a single test. This multiplexing capability enhances diagnostic accuracy and provides a more comprehensive assessment. Biosensors reduce health care costs as it does not require expensive diagnostic procedures, and lengthy laboratory processing times. Biosensors can be combined with advanced technologies like microfluidics, nanotechnology, or imaging techniques to enhance their performance and capabilities in cancer detection. All of these features collectively contribute to the potential for early and efficient cancer diagnosis, marking biosensors as a significant advancement in the field of medical diagnostics [53].

2.5. QCM Biosensor

2.5.1. Definition of QCM Biosensor

Piezoelectric biosensors occupy a prominent role in biochemical sensing within current biosensor systems. Devices within this category, exemplified by the QCM biosensor, leverage the piezoelectric crystal's resonance sensitivity to perceive alterations in the surrounding environment. In the realm of piezoelectric sensing, the QCM biosensor has emerged as the most prevalent, high-resolution technique for mass sensing, quick-response time, mass-sensitive, cost-effective, and simplicity. It employs a combination of simple and convenient converter receptors with biological recognition elements, which convert biochemical or biological responses into measurable output signals making it a versatile system for various applications. The QCM biosensor is a highly sensitive device that detect alterations in the quartz crystal's resonance frequency (Δf). The addition of any mass to biosensor resonator induces a shift in the resonator's oscillation frequency. Consequently, the detection of chemical interactions or biomolecular becomes achievable by measuring (Δf), directly correlating with the alteration in mass on the resonator surface as biomolecule binding increases mass and inversely affects oscillating frequency. These

systems allow precise measurement of resonance frequency by adjusting mass or thickness (Δm) on the crystal surface [54-59].

In contrast to traditional methods, these biosensors present numerous advantages, such as streamlined data analysis, detection without labels and in real-time, portability, compatibility with modern technologies, and affordability. Therefore, they are suitable for a variety of purposes, including environmental pollutant detection, disease diagnosis, protein quantification, and applications like DNA sensors, enzyme sensors, immunosensors with antibody functionalization, as well as sensors incorporating nanoparticles, cells, or microorganisms. The QCM biosensor is crucial in detecting of a diverse array of biomolecules, making it effective analytical tools. Their notable sensitivity and specificity establish them particularly promising for the identification of cancer cell [55-58, 60].

2.5.1.1. The Key Components of QCM Biosensor

Quartz crystal resonator is the primary element of the QCM biosensor: Typically, it is configured as a thin disk or plate composed of quartz or a similar material. This crystal generates an electrical charge through mechanical stress. The second element is the Electrode: It is usually made of metallic materials such as gold or silver, which is deposited on both surfaces of the quartz crystal in a QCM biosensor setup. These electrodes function as links for applying alternating electric fields and measuring resulting electrical signals. Next, the third element is the Sensing layer: A thin film or coating is applied to the quartz crystal's surface, selectively designed to interact with specific target molecules or analytes. This sensing layer may include biomolecules such as antibodies or enzymes, forming connections with the target molecules. The fourth integral element is the Oscillator circuit: Within the QCM biosensor, an oscillator circuit is integrated, generating a high-frequency Alternating Current (AC) voltage and directing it to the quartz crystal. The AC voltage frequency is typically in the megahertz range, such as 5 MHz or 10 MHz. The fifth part is the Measurement electronics: The QCM biosensor includes electronics responsible for monitoring and analyzing changes in the quartz crystal's electrical properties. These electronics typically consist of a frequency counter to gauge changes in frequency resulting from the adsorption or desorption of mass on the crystal's surface. The sixth element is data output and analysis: The measurement electronics link to a computer or data acquisition system that records the frequency

changes and enables data analysis and interpretation. This data can be used to determine properties such as mass of the adsorbed substance [54].

2.5.2. Principle and Operation of QCM Biosensor

By observing the changes in resonant frequency, the QCM biosensor can provide valuable information about the presence, concentration, or behavior of target substances. It enables real-time and sensitive detection of mass changes or alterations in the viscoelastic properties of the crystal's surface, making it highly valuable in diverse fields such as biosensing, material science, and chemical analysis.

The operation of the QCM biosensor device involves a series of interconnected processes. First, due to the piezoelectric effect in quartz crystals, when any mechanical stress is applied, an electrical charge is generated in response to it, and vice versa. This property facilitates the conversion of electrical signals into mechanical vibrations and vice versa, enabling a bidirectional transformation. Next, applying an alternating electric field to the quartz crystal induces vibrations at its resonant frequency, the natural frequency at which the crystal vibrates. A sensing layer coats the surface of the crystal designed to interact with specific substances, causing changes in mass when these substances bind to or interact with the sensing layer. These mass changes, in turn, affect the vibrational behavior of the crystal, leading to changes in the (f). As shown in the Figure 2.2 an increase in (m) leads to a decrease in the (f), whereas a decrease in (m) results in an increase in the (f). The frequency changes are measured through an oscillator circuit and converted into measurable signals, providing real-time information about the ongoing change in mass on the surface of the crystal. This comprehensive process allows for the continuous monitoring and analysis of biochemical interactions or other target substance detections [54, 61, 62].

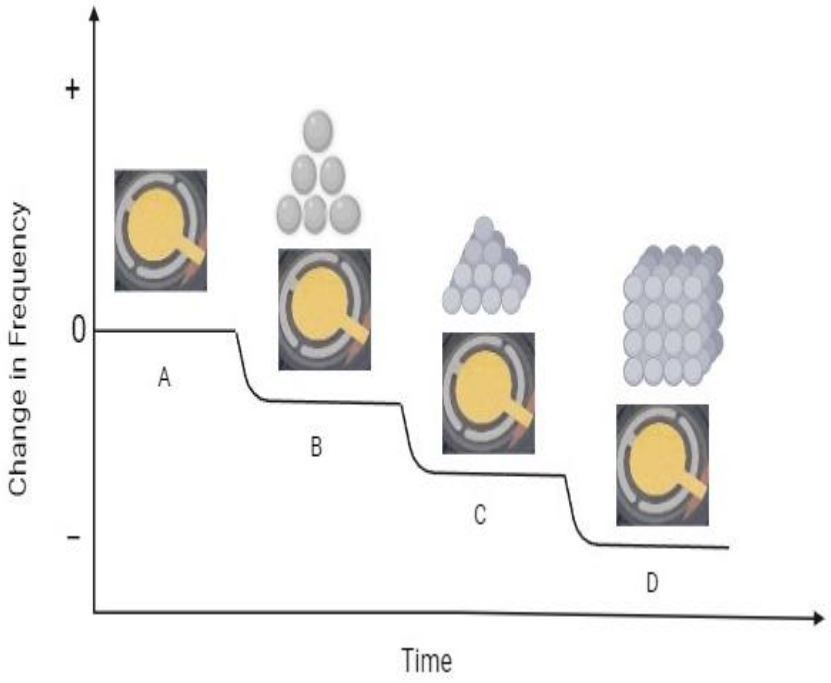

Figure 2.2. QCM biosensor principle. This image adapted from [61], and has been modified to highlight key features.

2.5.3. Types of QCM Biosensor

Various types of QCM biosensor are available, each designed for specific applications. There are two types according to the number of electrodes, and there are two types according to the method and angle of cutting the crystal:

1. Single Electrode QCM biosensor represents a fundamental form, consisting of a quartz crystal with a sensing layer on one side and a single electrode on the other. It is commonly used for simple mass measurements and easy integration into various systems [63].
2. Dual Electrode QCM biosensor introduces an enhanced design with two electrodes positioned on opposing sides of the quartz crystal. This dual-electrode configuration offers versatility for more complex analyses while maintaining the simplicity and adaptability inherent in QCM biosensor [64].

The orientation and angle of the cuts are crucial in determining the properties of the resulting sensor. As shown in the Figure 2.3, two common crystallographic planes used in the cutting of quartz crystals are the Analog Transverse (AT) and Blank Transverse

(BT) planes. These planes are defined based on the crystallographic structure of quartz [50, 65].

1-AT-Cut: In an AT-cut, the crystal is typically oriented at an angle of 35° and 15 minutes (35°15') from the Z-axis. This cutting is often used in devices like quartz crystal oscillators and resonators.

Properties:

- Good temperature stability.
- Suitable for applications requiring precise frequency control.

2-BT-Cut: in this case, the angle is -49.00°, meaning 49° from the Z-axis in the opposite direction. BT-cut is often used in sensor applications, including pressure sensors and accelerometers.

Properties:

- Good frequency stability with temperature changes.
- Suitable for sensing applications where stable performance across temperature variations is essential.

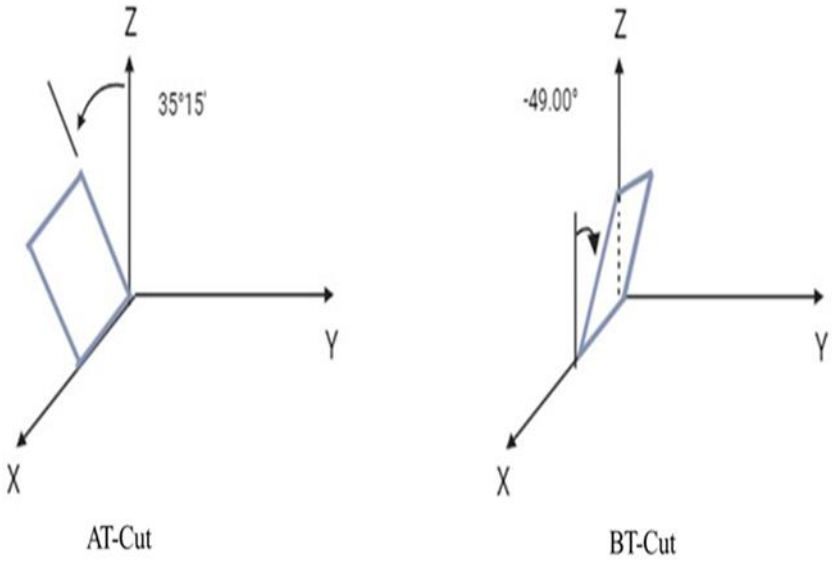

Figure 2.3. AT-cut and BT-cut of quartz crystals. The original image, from [66], has been adjusted for better visualization.

2.5.4. QCM Biosensor For Cancer Detection

QCM biosensor is a highly promising technology for detecting and diagnosing cancer. This biosensor features a design that incorporating a quartz crystal resonator coated with a thin layer of recognition elements like antibodies, that specifically target cancer biomarkers. These biomarkers can be proteins, or other cancer-associated molecules. Upon introducing a specimen (such as blood or tissue extract) to the sensor, the cancer biomarkers within the sample bind to the sensor's surface recognition elements. This binding results in a mass loading on the sensor, causing a shift in the (f). This frequency alteration is directly proportional to the amount of bound biomarkers. Electronic circuits connected to the QCM biosensor device detect and measure this frequency shift, providing quantitative information about the presence and concentration of cancer biomarkers. The obtained frequency shift data is further processed and analyzed to determine the specific cancer biomarkers present in the sample. By comparing the measured data with known biomarker profiles, it becomes possible to identify the type and stage of cancer or monitor treatment responses [66-68].

2.5.4.1. Advantages of QCM Biosensor for Cancer Detection

QCM biosensor possesses exceptional sensitivity, enabling the discovery of cancer biomarkers even at extremely low concentrations. It holds paramount importance in early cancer detection, especially when biomarkers might exist in minuscule quantities. One significant benefit is their capacity for label-free detection, removing the necessity for fluorescent or radioactive labels. One key advantage is their ability to detect without the need for labeling, which eliminates the need for fluorescent or radioactive labels and simplifies the assay process, thereby reducing costs. QCM biosensor provides real-time measurements, enabling continuous monitoring of biomarker interactions. This is particularly advantageous for studying dynamic processes such as biomarker binding kinetics and enables the capture of time-dependent changes in cancer biomarker levels. The biosensors exhibit versatility, detecting a wide range of cancer biomarkers, supporting multiplexed analysis for a comprehensive disease understanding and enhancing diagnostic accuracy. QCM biosensor provides relatively fast detection times, allowing for prompt analysis of cancer biomarkers. This is advantageous for timely decision-making in clinical settings, potentially leading to swift interventions and improved patient outcomes. Furthermore, their potential for miniaturization makes them

well-suited for point-of-care applications, enabling direct cancer detection at the point of care. This approach brings diagnostic capabilities directly to patients, particularly in settings with limited resources or remote locations, enabling early interventions [12, 67, 68].

2.5.4.2. Limitations of QCM Biosensor for Cancer Detection

The success of the QCM biosensor in detecting cancer biomarkers relies on the specificity, availability, and accuracy of its recognition elements, which are typically antibodies. However, challenges arise from interference in complex biological samples like blood or tissue extracts, resulting background noise and non-specific binding that may impact accuracy. Designing and optimizing the QCM biosensor for specific biomarkers can be complex, prompting the need for advanced surface functionalization techniques, optimized assay conditions, and the integration of nanomaterials to enhance sensitivity and selectivity. Continued research and development efforts are crucial in overcoming these limitations and further improving the capabilities of the QCM biosensor for cancer detection. Ongoing efforts can lead to advancements in recognition element specificity, optimization strategies, interference reduction techniques, user-friendly designs, and robust clinical validation, contribute to the advancement of cancer detection technologies [12, 66].

2.5.5. The Potential of QCM Biosensor for Detecting CD44 Receptors

QCM biosensor exhibits substantial potential for detecting CD44 receptors, pivotal in various biological processes, including cancer progression and metastasis. QCM biosensor has been extensively explored for cancer detection in various research contexts, showcasing their versatility and effectiveness. For instance, a study focused on developing a highly selective QCM biosensor for breast cancer cell detection. Utilizing antibodies targeting the Notch-4 receptor and coated with P(HEMA-NPs), the biosensor demonstrated notable sensitivity, selectivity, and stability, offering potential applicability in cancer cell detection [57]. Another study strived to establish a specific QCM system for detecting breast cancer cells expressing HER2/neu. Employing a QCM chip coated with polymeric nanoparticles and functionalized with a HER2/neu antibody, the system exhibited a low detection limit and effective identification for breast cancer cells expressing HER2/neu, offering promise for detecting specific molecular markers in breast

cancer [69]. These studies collectively underscore the potential of QCM biosensor in diverse applications within cancer detection and diagnostics.

2.5.6. Previous Studies

Upon scrutiny of current studies dedicated to the detection of malignant melanoma, a prevalent theme emerges-namely, the utilization of biosensors as expeditious and efficacious diagnostic instruments for discerning crucial indicators associated with malignant melanoma. A comprehensive analysis of these studies, reveals a notable absence of research centered on the utilization of (QCM) biosensor. This biosensor, distinguished by its heightened sensitivity, commendable precision, and user-friendly attributes, has demonstrated its efficacy across diverse studies pertaining to cancer diagnosis through the discernment of specific biomarkers.

In light of this identified research gap, we propose a strategic solution to address this lacuna by proposing the development of a QCM biosensor subjected to modification through integration with a nano polymer and tethered to specific antibodies meticulously designed to selectively bind with CD44. Noteworthy literature confirms to the pronounced expression of CD44 on MM cells. A meticulous review of antecedent research exposes an absence of focus on CD44 detection in prior studies, with attention primarily directed towards Tyrosinase (TYR) and MAGE-1.

In contradistinction to preceding inquiries, our study aims to introduce the integration of QCM technology with the CD44 biomarker, marking an unprecedented venture in the realm of malignant melanoma detection. This innovative approach seeks to bridge an evident research gap and contribute novel insights to the domain of biosensor-based diagnostics for malignant melanoma.

Table 2.1. Previous Studies.

Biosensing method	Recognition unit	Target/Cell	Sample	LOD	Ref
Fluorescence	silicon-doped carbon quantum dots (Si-CQDs)	Tyrosinase (TYR)	human serum	0.041 U/Ml	[70]
Fluorescence	lucigenin fluorescence	Tyrosinase (TYR)	human blood	0.2 mu g/mL	[71]
Fluorescence	carbon quantum dots (CQDs)	Tyrosinase (TYR)	human serum	33.21 U/L	[72]
Electrochemical	Graphene oxide (GO) polymer modified with cobalt protoporphyrin (CoPP) GO-CoPP	cytoplasmic polyadenylate element-binding protein 4 (CPEB4)	human serum	0.074 pg mL^{-1}	[73]
Electrochemical	anti-MAGE-1	MAGE-1	human serum	130 fg/mL	[74]
Electrochemical	anti-MAGE-1	MAGE-1	human serum	0.0035 fg/mL	[75]

3. MATERIAL AND METHOD

3.1. Materials

Ethylene glycol dimethacrylate (EDGMA,98%), sodium dodecyl sulfate (SDS, 99≥%), hydroxyethyl methacrylate (HEMA, 97%), ammonium persulfate (APS, 98≥%), sodium bicarbonate ($NaHCO_3$, 99%), 11-mercaptoundecanoic acid (MUA), sodium bisulfite ($NaHSO_3$, 99%), N-hydroxysuccinimide (NHS), polyvinyl alcohol (PVA, 99%),), 3-aminopropyltriethoxy silane (APTES), Phosphate Buffered Saline (PBS), ethyl-3-(3-dimethylaminopropyl) carbodiimide (EDC), DF6392 antibody. The QCM chips were acquired from Maxtek Inc. New York, NY, USA. The chemicals were sourced from Sigma-Aldrich Co. in St. Louis, MO, USA. All other chemicals were in analytical grade and purchased from Merck A.G. (Darmstadt, Germany).

3.2. Preparation of Poly(HEMA) Nanoparticles

Poly(HEMA) nanoparticles (P(HEMA-NPs)) were synthesized and characterized using the mini-emulsion polymerization technique. The synthesis involved a three-phase system. The first solution consisted of 50 mL of deionized water, in which 50 mg of PVA and 50 mg of SDS were dissolved. The continuous phase was established by dissolving 93.5 mg (PVA) in 5 mL of deionized water (DI) to create the second solution. Following the full dissolution of PVA, 12.5 mg $NaHCO_3$, and 14 mg SDS were introduced into the solution. The third solution comprised 1.05 mL EDGMA and 0.5 mL HEMA in 50 mL of DI. The third solution was gently mixed with the second solution on a magnetic stirrer. The resulting mixture was homogenized at 50000 rpm for 15 min at room temperature using a (T10 Ika Labortechnik homogenizer) (Staufen, Germany), forming a mini-emulsion.

Polymerization initiation involved dissolving 50 mg of $NaHSO_3$ and 100 mg of APS in deionized water and placing them on a (Scilogex MX-S vortex mixer). The first phase, composed of the polymerization reactor, was mixed with the mini-emulsion and initiator. The mixture was incubated with shaking for a whole day (24 h) at 40 °C and 500 rpm. To remove surface active compounds, unreacted monomers, and initiators the prepared polymer was placed in a centrifuge for 20 min at 8500 × g (3000 rpm). The upper layer (which contains polymer nanoparticles) was separated from the lower layer. After that,

the process of washing the polymer with ethanol (99%) began. In order to achieve a homogeneous redistribution of the particles, the nanoparticle with ethanol was placed in a water bath in the ALEX Machine Ultrasonic Cleaner for 15 min. The nanoparticle solution was then centrifuged with ethanol for 45 min using a Beckman Coulter Optima L-100K Ultracentrifuge Type 40 rotor at 81085 x g (35000 rpm).

The nanoparticle was washed with alcohol twice, then the washing process with distilled water was repeated five times with the same procedure used with alcohol. Finally, for nanoparticle size measurements, the final pellet was dissolved in distilled water. The process was repeated until nanoparticles of appropriate size, known to enhance QCM chip sensitivity, were obtained, as previous studies. The properly sized nanoparticles were then employed in the modification QCM chip [57, 69].

3.3. Attachment of Polymeric Nanoparticles to the QCM Chip Surface

Before starting the modification process for the QCM chip surface, ethanol (70%), DI, and acidic piranha solution (H_2SO_4): (H_2O_2) in a ratio of 3:1 (v/v) were used in order to wash the chip and ensure that there are no any impurities on the surface of the QCM chip [69].

In this study, the goal was to detect MM cells via their CD44 receptors. The DF6392 antibody was used, which is an antibody that was manufactured in the laboratory in order to bind selectively and specifically to CD44 receptors present on the surface of MM cells. However, the QCM surface must first be modified and the antibody must be fixed to the QCM chip surface.

3.3.1. Surface Modification of the QCM Chip

3.3.1.1. Coating the QCM Chip with MUA

The QCM sensor's surface was modified using MUA which forms chemically stable, well-organized monolayers called self-assembled monolayers (SAM). As shown in Figure 3.1, the interaction between thiols and gold surfaces can form Au–S coordination bonds. Hydrogen atoms can either adhere to surfaces or be released from the surface as H_2. As a result of this reaction, the sulfhydryl group of MUA allows the MUA layer to bond to the gold surface [76].

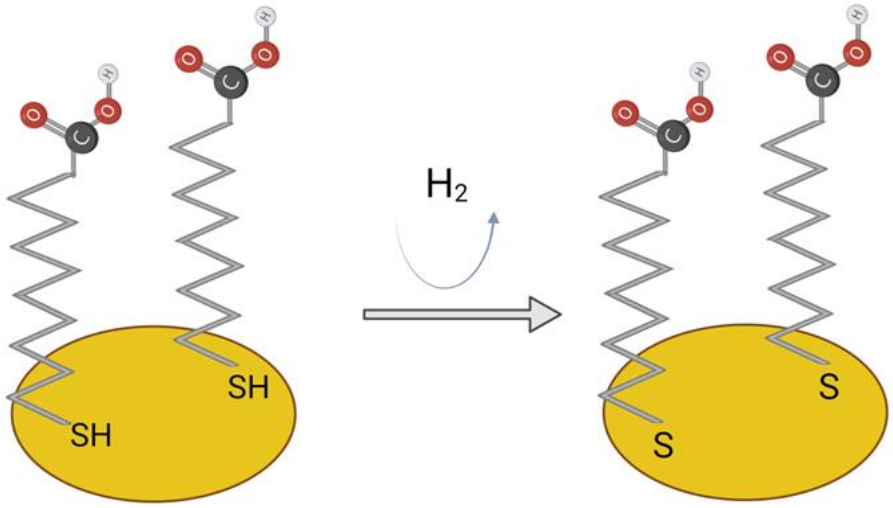

Figure 3.1. Coating the QCM chip with MUA. This illustration, obtained from [78], has been edited for clarity.

3.3.1.1.1. Prepare MUA Solution

To prepare the MUA solution, 11-mercaptodecanoic acid was obtained from Sigma-Aldrich. Next, to achieve surface modification of the QCM sensor using MUA, 1 mg/mL MUA (pH, 4.5) was dissolved in 5 mL of ethyl alcohol and the surface was exposed to the solution [76].

3.3.1.1.2. Application of MUA Coating Process

Quartz coating was performed under a sterile hood to prevent contamination. It was incubated with 100 μL of the MUA solution and left overnight at room temperature.

3.3.1.2. EDC/ NHS Crosslinking

EDC it is a chemical that contains biological substances that contain amines. It is the most popular carbodiimide used for conjugation. EDC with NHS, is almost universal in its application in particle and surface coupling processes. Incorporating NHS into EDC reactions offers the benefit of enhancing the solubility and stability of the active intermediate. Therefore, reactions combined with EDC/NHS are generally slower than those obtained with EDC alone. It also increases the coupling efficiency. A typical EDC/NHS reaction first results from the incorporation of EDC. The active O-acylisourea intermediate is formed as shown in the Figure 3.1. Later, the addition of NHS stabilizes the reactive amino intermediates by converting the EDC to a succinimidyl ester. Thus, it facilitates the stabilization of biosensor elements through the formation of a covalent bond [77, 78].

3.3.1.2.1. Prepare EDC/NHS Solution

In the literature, the concentration ratio between EDC and NHS is generally 1:1 and a concentration of 5 mg/mL is used. In these trials, EDC and NHS were given separately. 5 mg of (pH, 6.5), (6 mM), EDC was dissolved in 1 mL of deionized water and vortexed for approximately 20 sec. The same procedures were applied to the second solution, 5 mg of (pH = 6.5), (45 mM), NHS was dissolved in 1 mL of deionized water and vortexed for approximately 20 sec.

3.3.1.2.2. Application of EDC/NHS Crosslinking

After the MUA coating process, in order to remove excess chemicals physically adsorbed on the surfaces, the QCM surface was washed with ethyl alcohol. After this process, EDC was administered onto the surface for 2 h, after that the same process was applied with the NHS.

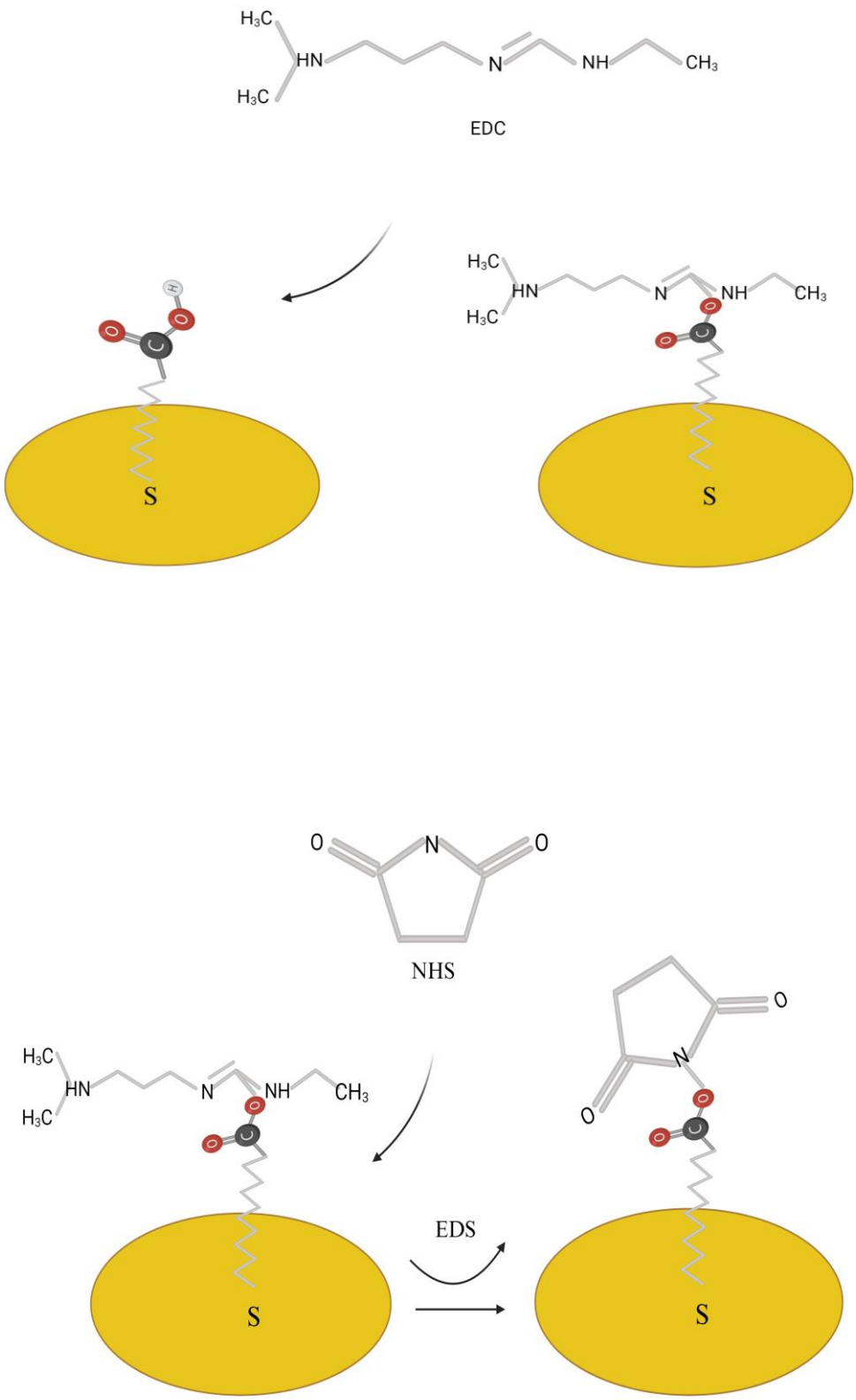

Figure 3.2. Application of EDC/NHS on a QCM chip modified with MUA. This image adapted from [74,78],and has been modified to highlight key features.

3.3.1.3. Functionalization of the P(HEMA-NPs) with APTES

A silanization agent (APTES) was used in order to activate P(HEMA-NPs). APTES 3-aminopropyltriethoxysilane, it is a silane coupling agent that contains an amino group (NH_2) and is commonly used to modify surfaces for various applications. APTES can bond to surfaces containing hydroxyl groups (-OH) through a condensation reaction, forming a stable and covalent linkage. As shown in the Figure 3.3, and Figure 3.4, we used APTES to modify the surface of the HEMA polymer to introduce amino groups, this amino group is used to bind the P(HEMA-NPs) to the surface that was modified with MUA because the carboxylic acid group in the MUA, which was activated using EDC/NHS, binds better to the amine group rather than to the hydroxyl group that was present on the surface of the P(HEMA-NPs).

For this, the P(HEMA-NPs) synthesized were mixed with 200 µL of silane reagent (0.9%), Then the solution was positioned on a magnetic stirrer for (24 h). Leaving the solution on a magnetic stirrer for a whole day allows for sufficient reaction time between the P(HEMA-NPs) and APTES. This duration ensures the functionalization of the nanoparticle surface with amino groups.The solution was centrifuged at 3000 rpm for 20 min to separate the modified nanoparticles from any unreacted APTES or other by-products. It was then rinsed with ethanol to eliminate any residual APTES and impurities and then placed in a sonicator until homogeneous for 40 min. Then it was added to the surface of the sensor chip [79].

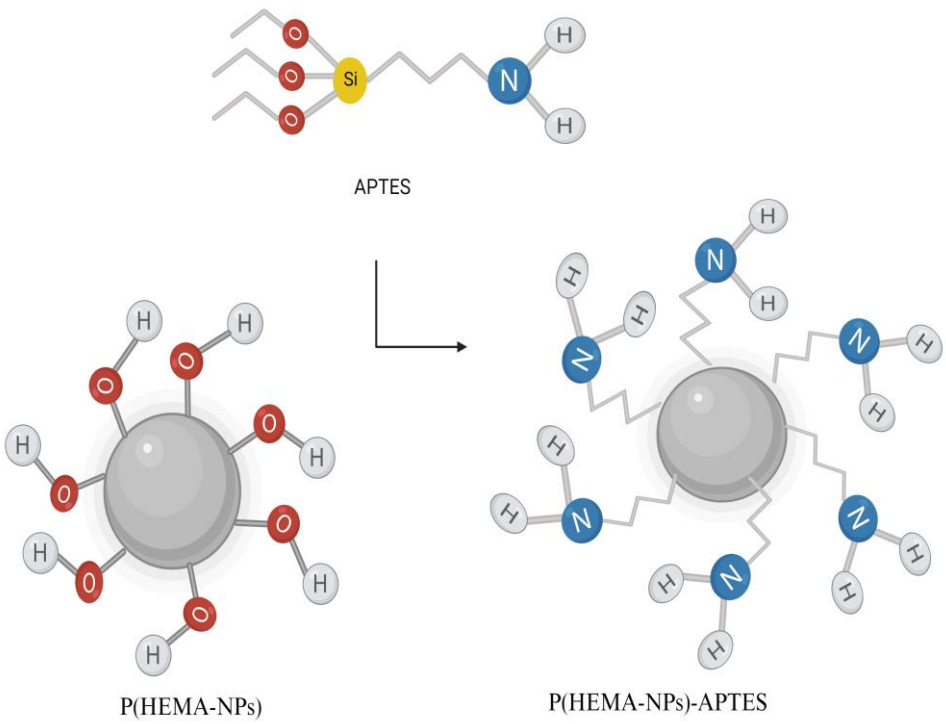

Figure 3.3. Functionalization of the P(HEMA-NPs) with APTES. This image was sourced from [79] and subsequently modified.

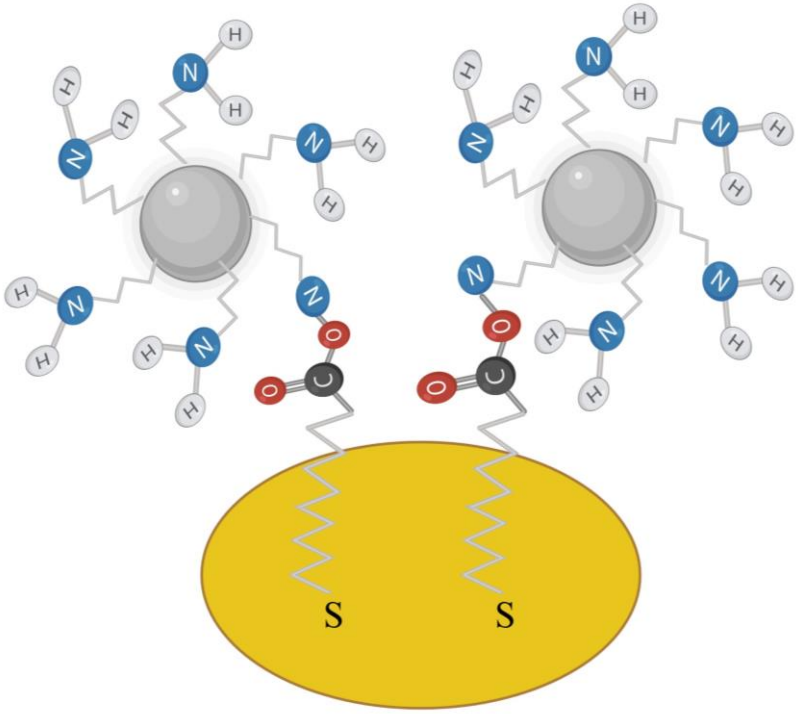

Figure 3. 4. Application of P(HEMA-NPs)-APTES on a QCM chip modified with MUA. The original image from [79], has been adjusted for better visualization.

3.3.1.4. Modification of DF6392 Antibodies

EDC/NHS are combined to activate carboxylic acid groups, preparing them for subsequent conjugation with amino groups. We utilized it as a bioconjugation technique to activate the carboxylic acid group in the DF6392 antibody, facilitating its binding to the amine group on the P(HEMA-NPs) modified with APTES, thus forming stable amide bonds.

EDC is a zero-length crosslinker that activates carboxylic acid groups. It works by converting carboxylic acid groups to an O-acylisourea intermediate, which can then react with amino groups. EDC is often used in combination with NHS to enhance the reaction efficiency. NHS is often used in conjunction with EDC. It reacts with the intermediate formed by EDC, replacing the labile O-acylisourea group with a more stable NHS ester. This NHS ester is reactive towards primary amines, forming stable amide bonds [80].

3.3.1.4.1. Immobilization of Antibodies on the QCM Chip

The concentration ratio between EDC and NHS is 1:1 and a concentration of 5 mg/mL is used. The EDC solution was vortexed for approximately 20 sec. The same procedures were applied to the second solution, Next, the EDC/NHS solution was introduced into the DF6392 antibody solution then stirred the mixture immediately to ensure thorough mixing and even distribution of the activating agents (400 rpm). After 2h, we added the mixture to the P(HEMA-NPs) modified with APTES and placed on the surface modified with MUA. Thus, the carboxylic acid group present in the DF6392 antibody, which was activated using EDC/NHS, was bound to the amine group present on the modified polymer as shown in the Figure 3.5.

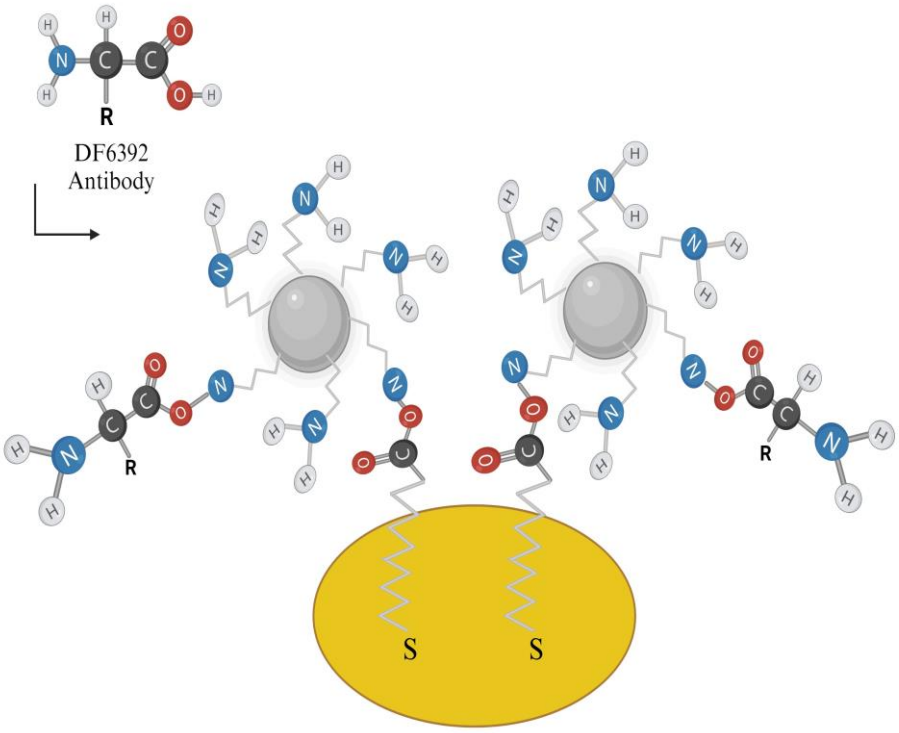

Figure 3.5. Immobilization of DF6392 antibodies on the modified QCM chip. Adapted from [78], this figure has been updated for clarity and accuracy.

3.4. Characterization Studies

The surface binding of cells, which forms the sensing component of the QCM biosensor, was thoroughly characterized through a combination of physical and chemical analyses applied to both QCM chip surface and nanoparticles.

3.4.1. Characterization of Nanoparticles

3.4.1.1. Zeta-Size Analysis

The sizes of the nanoparticles were determined before attaching them to the surface of the QCM chip. Size analysis, encompassing parameters such as average size, and dispersion of P(HEMA-NPs), was conducted using a Nano Zetasizer. In brief, the measurements were taken by placing a 1 mL of P(HEMA-NPs) into the device at room temperature using light scattering and the process was repeated three times. Using Zetasizer analyzer software (NanoS, Malvern Instruments, London, UK), the results were analyzed and some values such as standard deviation were recorded.

3.4.1.2. FTIR-ATR Spectroscopy

The P(HEMA-NPs) were characterized using (Thermo Fisher Scientific, Nicolet İS10, Waltham, MA, USA) (FTIR-ATR). To minimize interference from humidity and carbon dioxide, nitrogen gas was passed through the sample chamber for 10 min. Subsequently, the polymer was positioned in the sample aperture of the instrument, and spectra were acquired by measuring the total surface reflection in the range of 400 to 4000 cm^{-1} for wavelengths. This was done twice, once for only the P(HEMA-NPs) and once for the P(HEMA-NPs)- APTES.

3.4.2. Characterization of Polymeric Nanoparticles Coated QCM Chip

3.4.2.1. Contact Angle Measurements

The contact angle of the surface of the unmodified QCM chip was evaluated to ascertain its hydrophilic properties using (Hamburg, Germany) KRÜSS DSA100 device. Five distinct locations on the unmodified QCM chip surface were selected, and a water droplet was deposited on each site. Measurements of contact angles on both sides of the droplet were averaged. The same procedure was conducted on modified QCM with MUA, QCM modified with MUA and P(HEMA-NPs)-APTES and QCM modified with MUA and Ab-NPs. For contact angle values, the average values of five measurements were calculated. Measurements were made by the sessile drop method.

3.4.2.2. Atomic Force Microscopy (AFM)

The unmodified QCM chip, QCM modified with MUA, and QCM modified with MUA and APTES- P(HEMA-NPs) underwent analysis using (Nanomagnetics Instruments, Oxford, UK) (AFM). AFM can capture measurements at a very high resolution, specifically 4096 x 4096 pixels, utilizing its free cantilever interferometer feature. For weather imaging studies, the QCM sensor was affixed to the sample holder using double-sided carbon tape. The imaging process was executed in a tapping mode within the environment, with an oscillation resonance frequency of 341.30 kHz applied. An image covering an area of (2 x 2) µm was acquired at a scanning speed of 2 µm/s, featuring a resolution of (512 x 512) pixels.

3.5. Real Time Cell Detection

Following the modification of the sensor surface, attachment of the P(HEMA-NPs), and modification with the DF6392 antibody, kinetic studies were subsequently initiated. The surface of the QCM coated with Ab-NPs was rinsed with deionized water. After that, to equilibrate the surface and absorb unbound antibody molecules, 0.1 M NaCl was passed, then (pH, 7.4) (phosphate buffered saline) PBS was passed in order to eliminate of any excess NaCl, the solutions were passed onto the QCM chip surface using a Watson Marlow Sci 400 peristaltic pump at a speed of 0.5 mL /min. For 3 min the PBS was passed in order to prepare the QCM chip for measurements. It was balanced at room temperature and the resonance frequency (f) was determined. After this equilibration step, A375 cell solutions of different concentrations(50-5000) cells/mL were introduced into the system one by one (5 mL, flow rate of 1 mL/min). The shift values at the resonant frequency were observed immediately. When it reached equilibrium (about 1h), adsorption was performed by administering a 1M NaCl solution to the system. After adsorption, the QCM sensor was washed again with water and PBS. MAXTEK RQCM Inficon (Quartz Crystal Microbalance Monitor) was used for all analyses.

As shown in the Figure 3.6, the QCM system comprises an oscillator circuit, frequency counter,voltage source, peristaltic pump, isolation cabinet and computer interface.

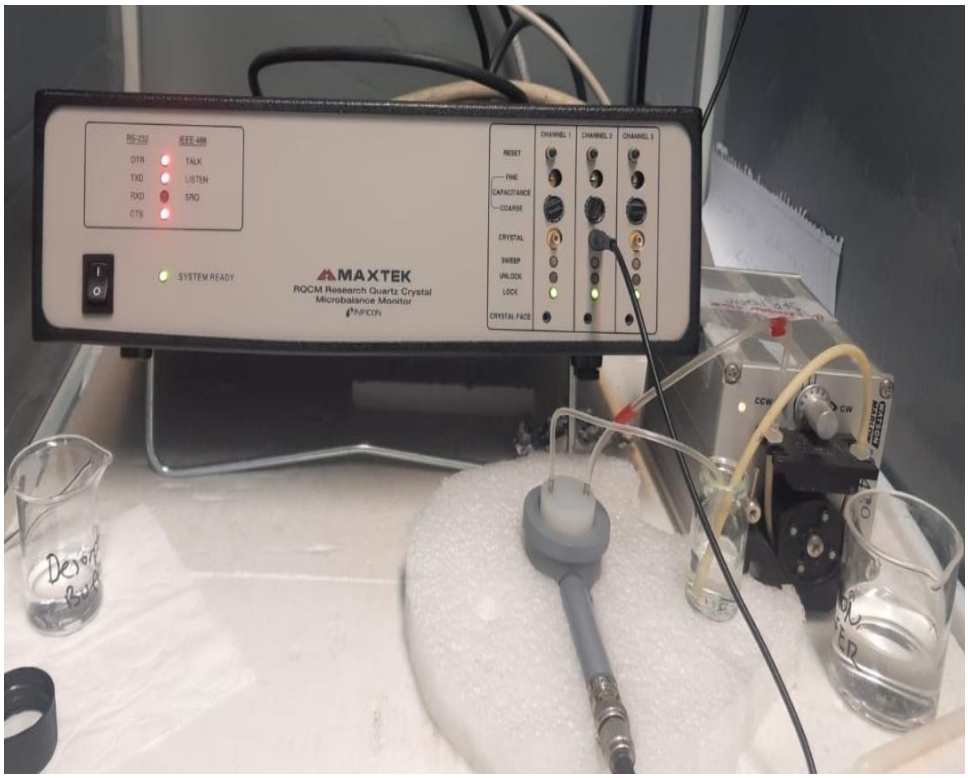

Figure 3.6. QCM system components.

The Sauerbrey equation, relying on the physical and geometric characteristics of quartz crystal, was employed to convert (f) into (m), Sauerbrey shows the linear correlation between Δf and Δm.

In this equation, (f_0) it symbolizes the resonance frequency of the fundamental mode, (A) piezoelectrically active gold disk area, (ρ_q) density of quartz, (Δm) surface mass loading, (μ_q) shear modulus, and the mass increase per unit of area (Δm/A)

$$\Delta f = - (2 f_0^2) * \Delta m / A\sqrt{\rho_q * \mu_q} \quad \text{.....(1)}$$

3.6. Selectivity Studies

For evaluating the selectivity of the QCM chip functionalized with Ab-NPs, kidney cancer cells HEK293 and pancreatic cancer cells PANC-1 were used, which contain a very small amount of CD44 compared to MM cancer cells (A375), which contain the largest percentage of CD44. 2500 cells/ mL were administered onto the surface of the QCM chip. After that change in frequency and mass was recorded for each of them.

3.7. Reusability Studies

The QCM coated with Ab-NPs was reused multiple times to assess both its stability and reusability. The same concentration of cells was passed three consecutive times, and the change in frequency and mass for each of them was recorded to confirm its ability to be repeated.

4. RESULTS AND DISCUSSION

4.1. Nanoparticle Characterization

4.1.1 Zeta-Size Analysis of P(HEMA-NPs)

In Figure 4.1, the results of the analysis of P(HEMA-NPs) zeta size prepared with EDGMA cross-linker and HEMA monomer can be observed. We obtained a polydispersity index of 0.373 nm and 90.29 nm was the average nanoparticle size.

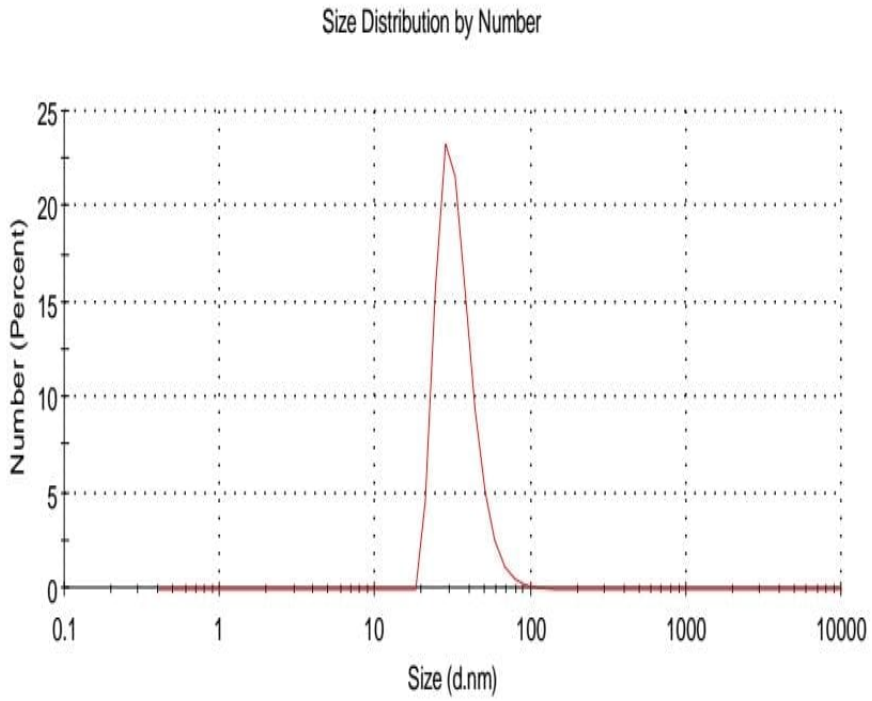

Figure 4. 1.Zeta size analysis of P(HEMA-NPs).

4.1.2. FTIR-ATR Analysis of the P(HEMA-NPs)

We modified the P(HEMA-NPs) using APTES to replace the hydroxyl group with an amine group. This modification was carried out to facilitate strong bonding with carboxyl group present on the QCM surface, which had been previously modified with MUA. FTIR-ATR was utilized for the characterization of both P(HEMA-NPs) and -P(HEMA-NPs)- APTES. FTIR is a powerful analytical technique used for identifying functional groups in a given material by measuring the absorption of infrared radiation. The nanoparticles was placed in the sample slot of the device, and the total reflection amount occurring on the surface were measured. The FTIR analysis provided important information into the chemical composition and structural modifications of the P(HEMA-NPs) before and after modification with 3-aminopropyltriethoxysilane (APTES). The obtained spectra revealed distinctive peaks associated with specific functional groups, allowing for a comprehensive characterization for polymers.

As shown in Figure 4.2, the FTIR-ATR spectrum of the P(HEMA-NPs) is depicted. The FTIR spectrum exhibited characteristic peaks consistent with its molecular structure. The presence of a broadband within 3000-3700 cm^{-1} indicated the stretching vibrations of the hydroxyl (-OH) groups. Additionally, a strong peak at approximately 1722 cm^{-1} was observed, corresponding to the (C=O) carbonyl group. The peaks in the region 1000-1400 cm^{-1} represent the (C-O) in the hydroxyl groups. The spectrum also exhibited peaks corresponding to (C-H) stretching vibrations around 2850-3000 cm^{-1}. These values indicate the completion of the polymerization process [81].

Figure 4.3 shows the FTIR-ATR spectrum of the P(HEMA-NPs)- APTES. The spectrum for P(HEMA-NPs)-APTES demonstrated notable changes, confirming the success of the grafting process. A new peak in the range of 1000-1100 cm^{-1} pointed to the existence of (Si-O-Si) siloxane linkage, indicating the integration of APTES into the polymer structure. Additionally, the appearance of peaks around 3300-3500 cm^{-1} suggested the introduction of amino groups (NH_2), further supporting the successful modification [81].

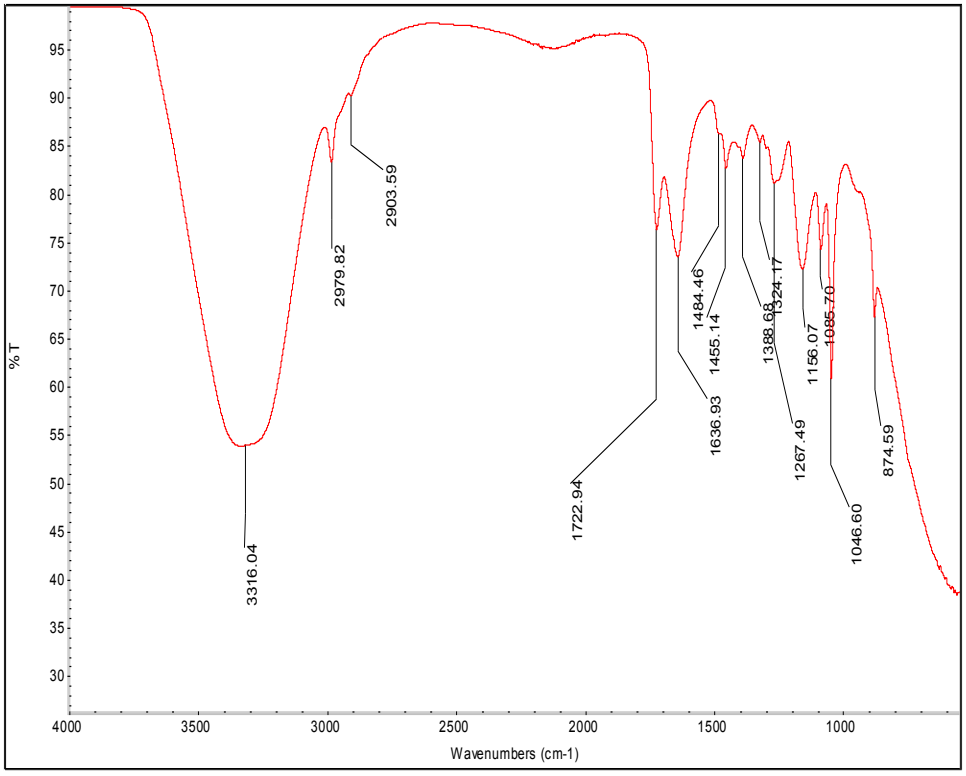

Figure 4. 2. FTIR-ATR spectrum of the P(HEMA-NPs).

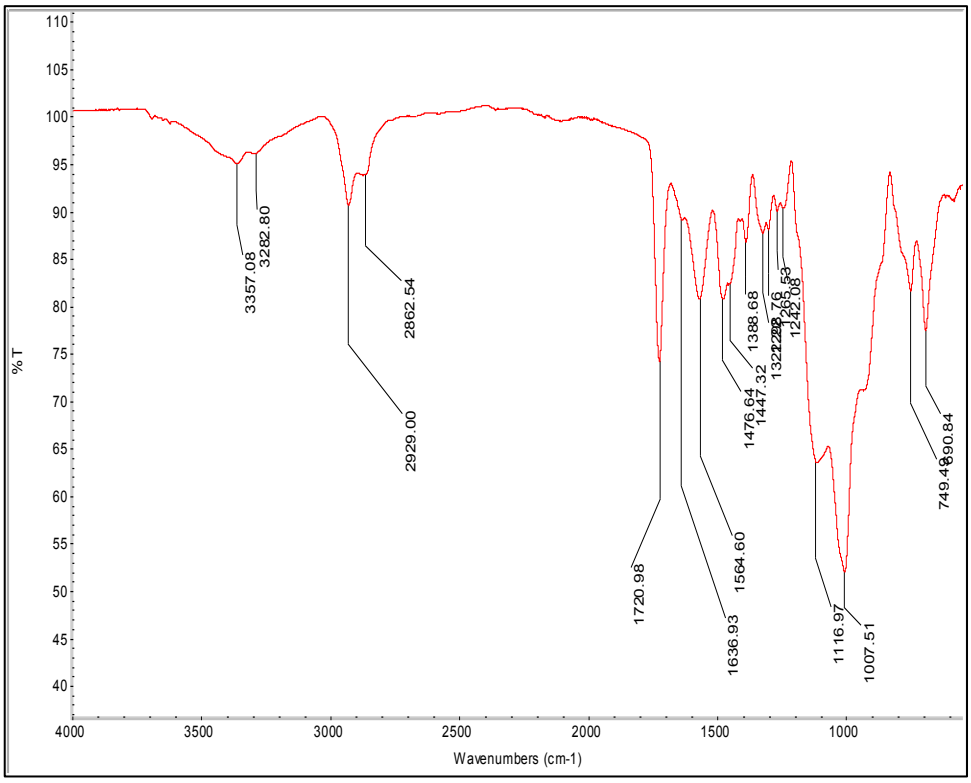

Figure 4. 3. FTIR-ATR spectrum of the P(HEMA-NPs)-APTES.

These findings align with the expected outcomes of the APTES modification reaction, where the ethoxy groups from APTES react with the hydroxyl groups present in polymer, leading to the formation of siloxane linkage and introducing amino groups. The FTIR analysis served as a powerful tool for elucidating these structural changes, providing critical information for the characterization of the modified polymer.

4.2. Characterization of QCM chip

4.2.1. Contact Angle Measurements

The unmodified QCM chip, QCM modified with MUA, QCM modified with MUA and APTES-P(HEMA-NPs), and Ab-NPs QCM chip was characterized using the KRÜSS DSA100 contact angle device (Hamburg, Germany). Using DSA2 software, contact angle values were calculated.

Table 4.1. Surface contact angles for the QCM chip in all modification steps.

Surface	**Contact angle, °**
Unmodified QCM surface	93.0° ± 1.43°
QCM-MUA	70.6° ± 4.25°
QCM-MUA-(P(HEMA-NPs)-APTES)	64.6° ± 4.66°
QCM-MUA-(P(HEMA-NPs)-APTES)-Ab-NPs	39.9° ± 2.65°

The contact angle measurements provided crucial insights into the evolving surface properties. As shown in the Figure 4.4, (A) the initial contact angle of the empty QCM chip was measured at 93° ± 1.43°, indicative of the inherent hydrophobicity of the unmodified surface. Upon modification with 11-ercaptoundecanoic acid (MUA), a notable reduction in contact angle to 70.6° ± 4.25° was observed Figure 4.4 (B), signaling an increased hydrophilicity associated with the introduction of carboxylic acid groups. Subsequent modification with the P(HEMA-NPs), modified with (APTES), induced a substantial decrease to 64.6° ± 4.66° Figure 4.4 (C). This reduction suggests a synergistic effect of the hydrophilic P(HEMA-NPs) and the formation of siloxane linkages via APTES, significantly altering the surface properties. The final step, involving antibody addition, resulted in a decrease to 39.85° ± 2.65° Figure 4.4 (D), indicating successful

antibody immobilization. The amino groups introduced during the APTES modification likely played a crucial role in facilitating specific antibody binding. These systematic decreases in contact angles underscore the successful modification steps.

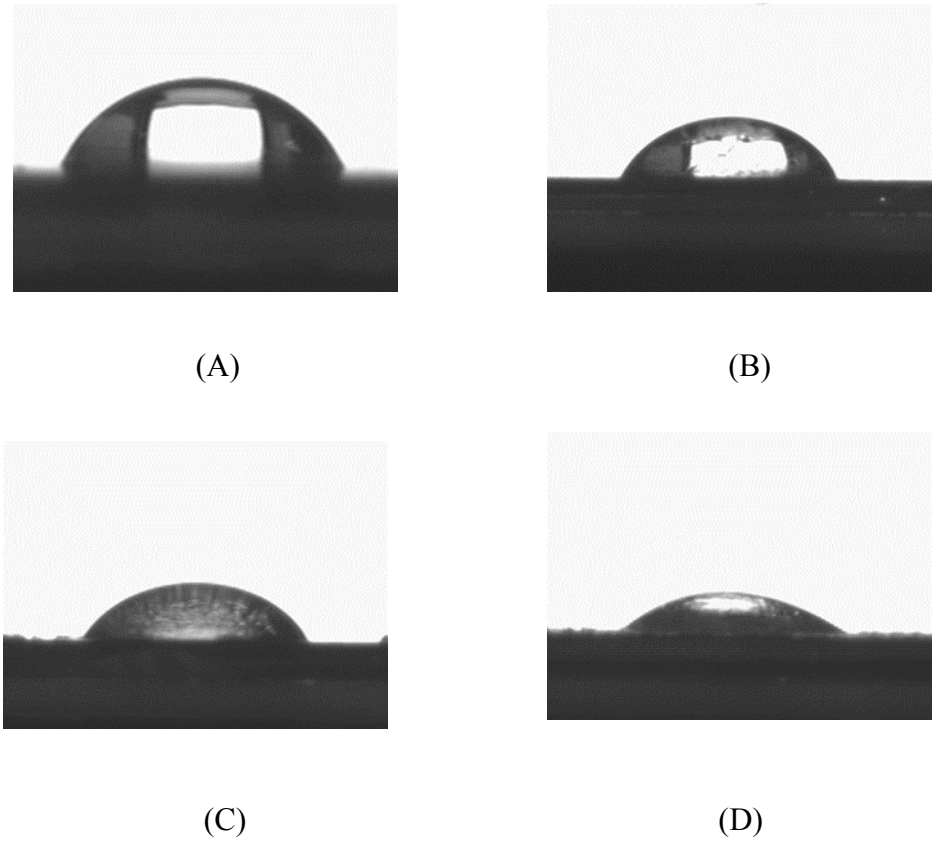

(A) (B)

(C) (D)

Figure 4. 4. Contact angle measurements of the (A) unmodified QCM chip, (B) QCM modified with MUA, (C) QCM modified with P(HEMA-NPs)-APTES, and (D) Ab-NPs QCM chip.

4.2.2. Atomic Force Microscope Analysis

The surface morphology of the unmodified QCM chip, QCM modified with MUA, and QCM modified with MUA and P(HEMA-NPs)-APTES was characterized using AFM measurements in tapping mode. When examining the unmodified QCM, the surface exhibited a relatively low roughness with a roughness average (Ra) of 0.265 nm, indicating a moderately smooth surface. Upon functionalization with MUA, we observed an increase in surface roughness, with Ra rising to 0.39 nm. This suggests the successful immobilization of MUA on the QCM, contributing to larger bumps and pits on the surface. Subsequent application of the P(HEMA-NPs)-APTES resulted in a significant increase in roughness, with Ra reaching 8.18 nm. It led to the formation of more prominent surface features, as evidenced by the higher Ra value. The negative skewness (-0.035) for the unmodified QCM shifted to a positive skewness (0.33) with the introduction of MUA and (0.52) with P(HEMA-NPs)-APTES, indicating a transition towards a more symmetric surface. These results indicate the successful attachment of P(HEMA-NPs)-APTES to the MUA -modified gold QCM surface (Figure 4.5, Figure 4.6, and Figure 4.7).

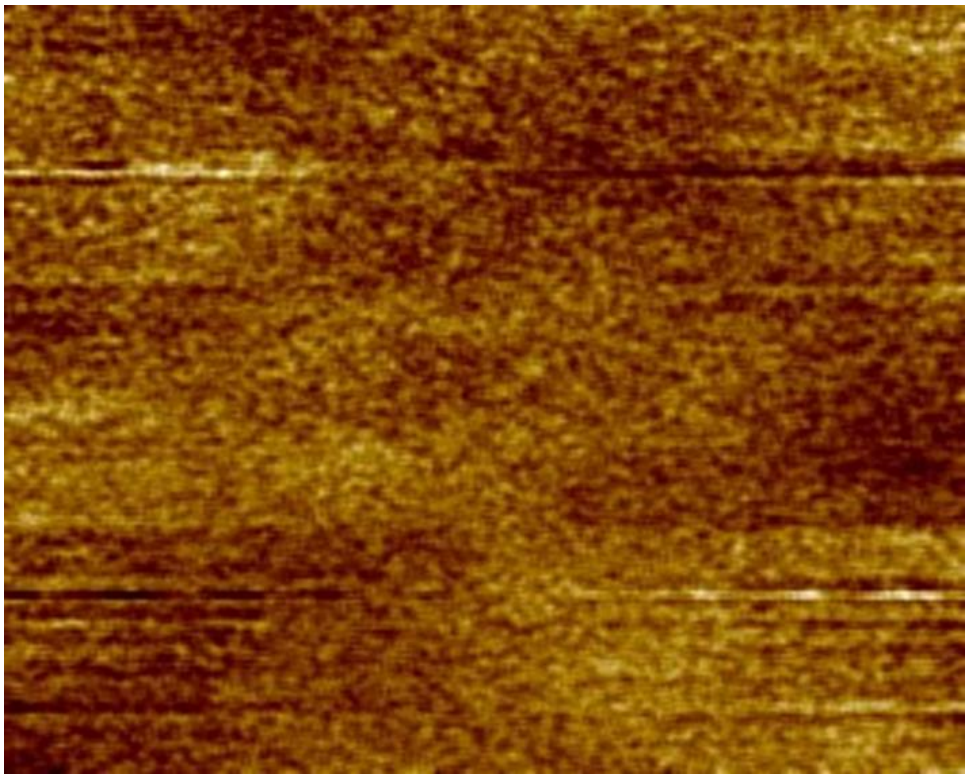

(A)

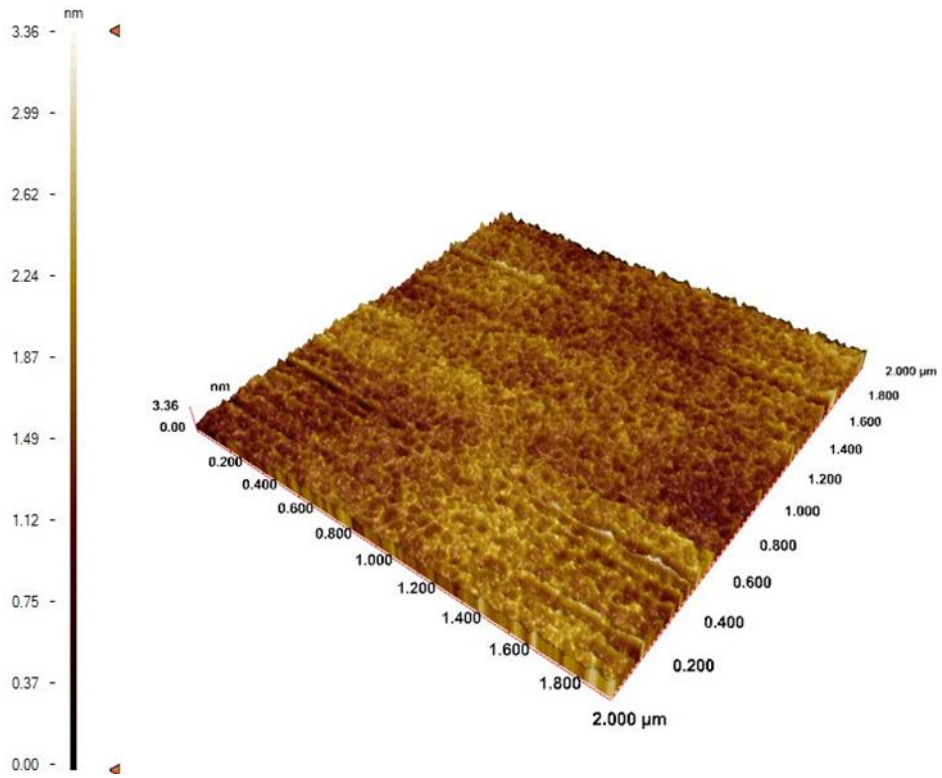

(B)

Figure 4. 5. The surface morphology of the unmodified QCM chip in 2D (A) and 3D (B).

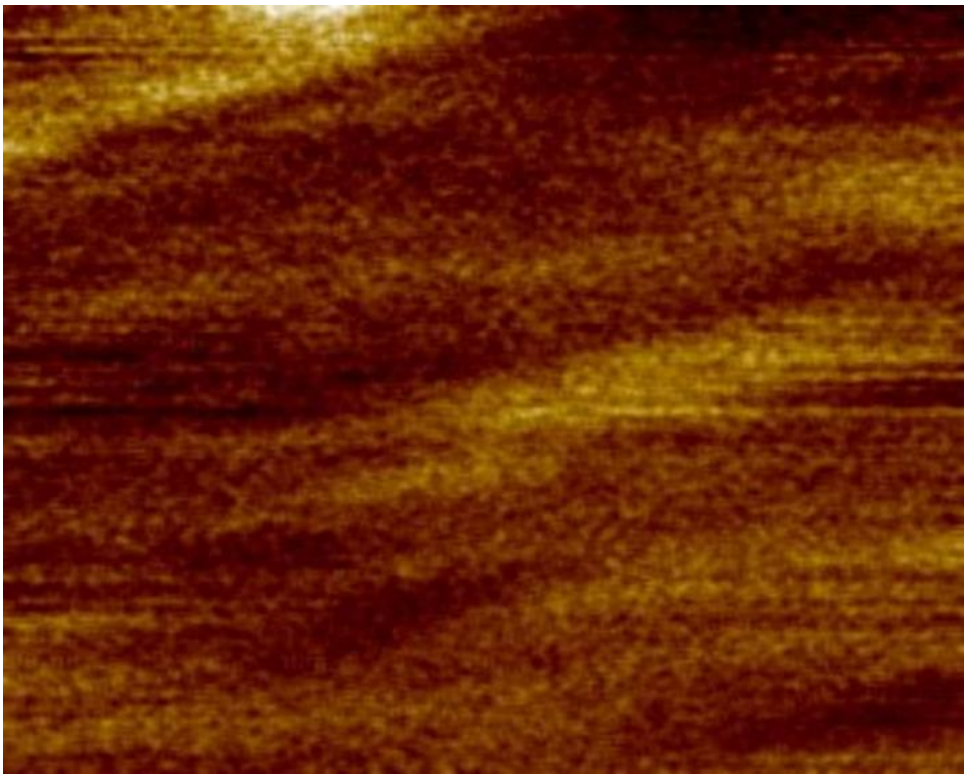

(A)

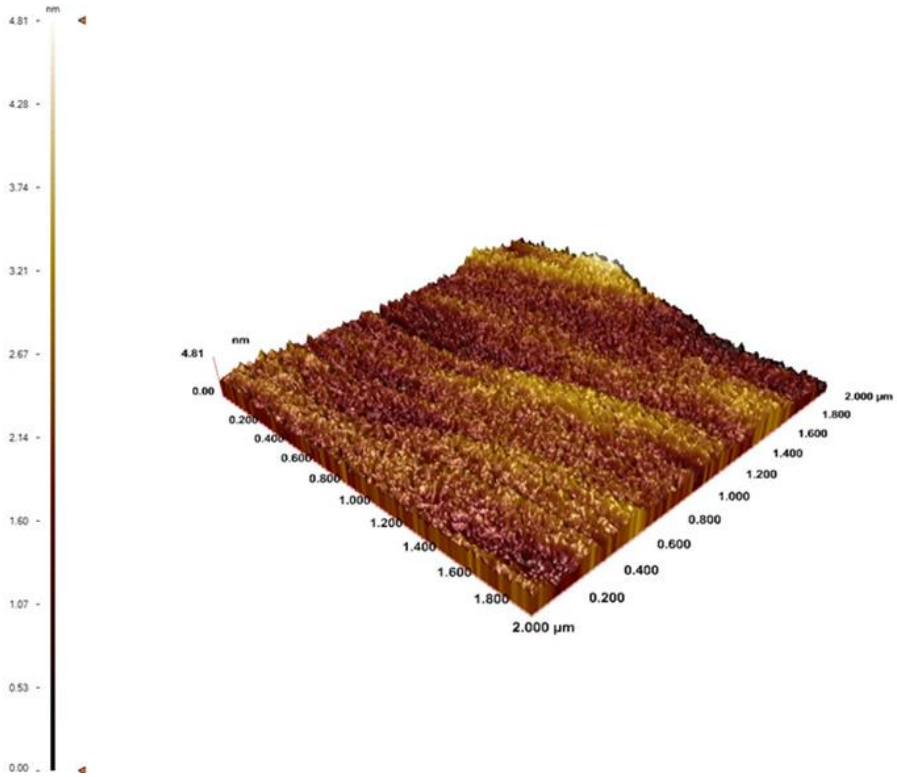

(B)

Figure 4. 6. The surface morphology of the modified QCM chip with MUA in 2D (A) and 3D (B).

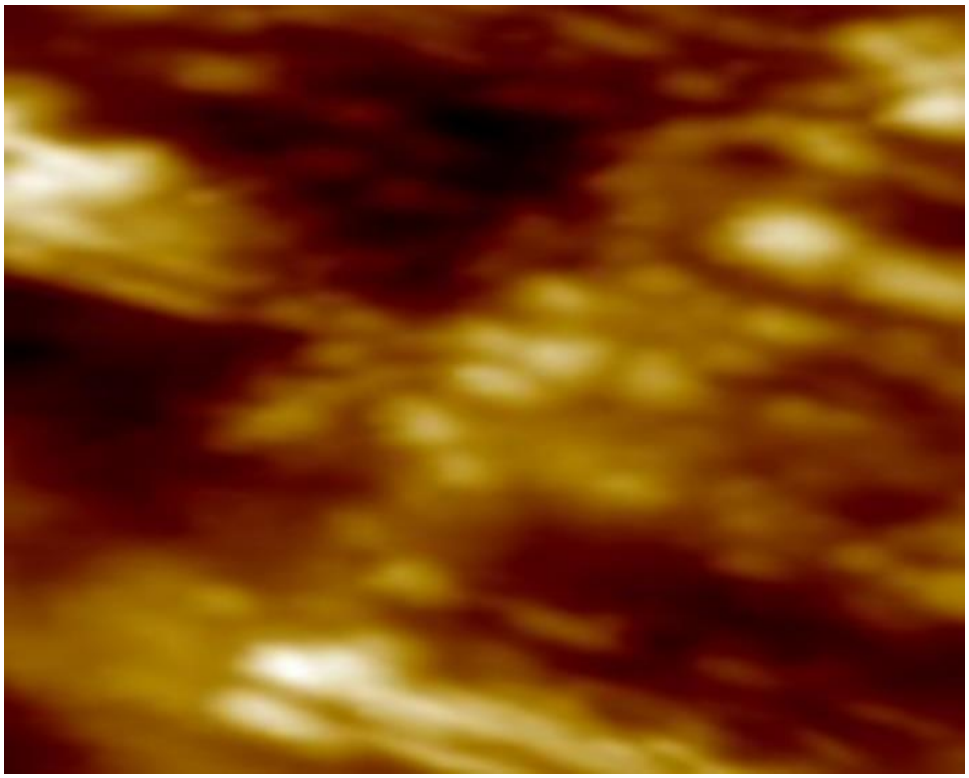

(A)

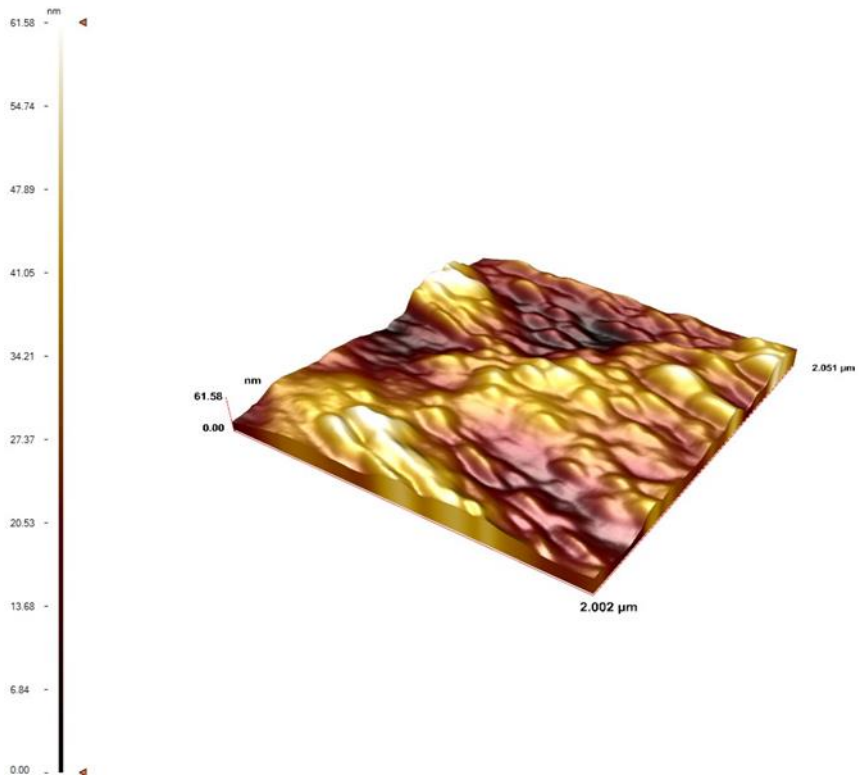

(B)

Figure 4. 7. The surface morphology of the MUA-modified QCM chip with APTES P(HEMA-NPs) in 2D (A) and 3D (B).

4.3. Real Time Cell Detection

QCM sensors were prepared using P(HEMA-NPs) modified with DF6392 antibody for selective detection of A375 cells. Cell solutions with different concentrations, (50-5000) cells/ mL was prepared to investigate the correlation between the QCM signal and the concentration of A375 cells. These solutions were interacted with QCM sensors using a peristaltic pump. The RQCM (Maxtek) software was used to monitor the obtained data in real-time and collect kinetic information. Sensorgram obtained from A375 cell solutions at different concentrations are presented in Figure 4.8 (Sensorgram showing the change in frequency (Δf (Hz)) over time) and Figure 4.9 (Sensorgram showing the change in mass (Δm (cell/mL cm^2)) over time).

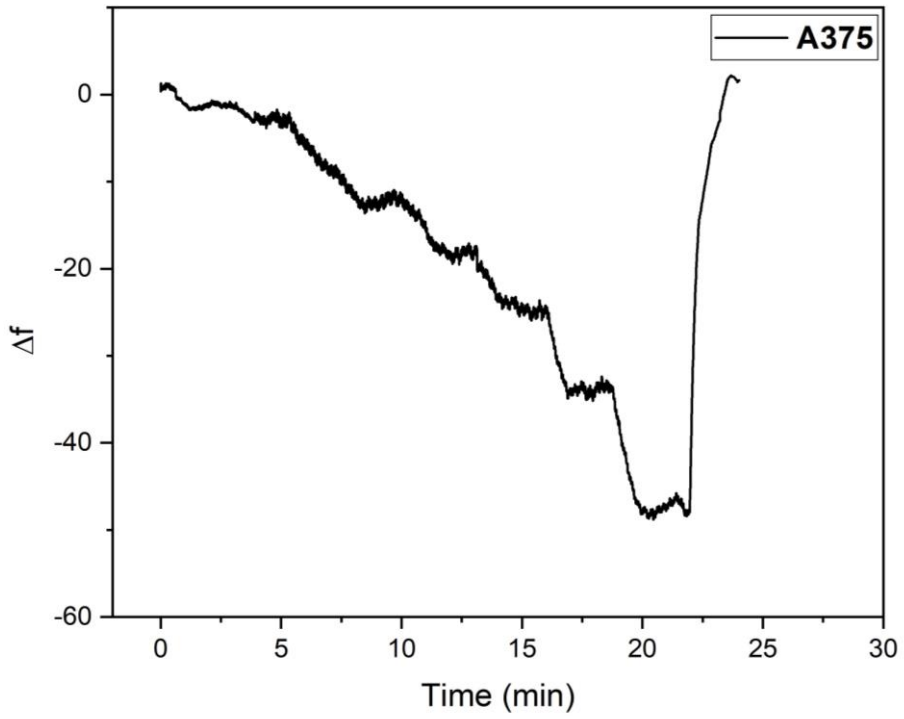

Figure 4. 8. The change in frequency (Δf) over time.

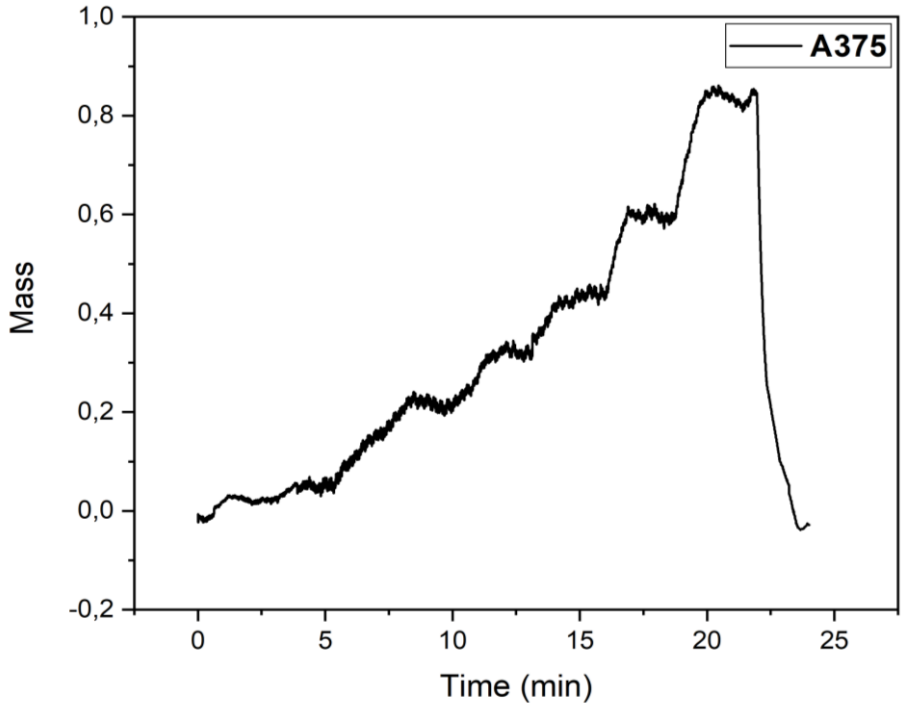

Figure 4. 9. The change in mass (Δm) over time.

In Figure 4.8, graphs illustrating the (Δf) over time, obtained by applying different A375 cell concentrations (50-5000) cells/mL, are presented. Additionally, Figure 4.9 provides graphs showing the (Δm) over time. In this manner, all the graphs for A375 cell solutions at different concentrations are presented together. In a standard measurement, the system was initially exposed to equilibrium buffer for 3 min. Subsequently, the cell solution was passed through the system until it reached a new equilibrium (approximately 30 min), and finally, a desorption solution was used (approximately 15 min). In all measurements, approximately 60 min were allowed for the system to reach equilibrium. As observed from the figures, the (Δf) and, (Δm) increase proportionally with the concentration.

İn Figure 4.10, the value of (f) decreases as the (C) increases. The QCM sensor shows linearity in the concentration signal within the range (50-5000) cells/mL. When these data were evaluated, the equation of the linearity obtained is calculated as (y = -0.0092 x - 5.2802), with a linearity (R^2) of 0.9619. From these data, we conclude that the equipped QCM sensor provides measurements with 96% accuracy. In Figure 4.11, (m) increases

with increasing (C), the equation of the linearity obtained is calculated as (y = 0.0001x +0.1531), with a linearity (R^2) of 0.8743.

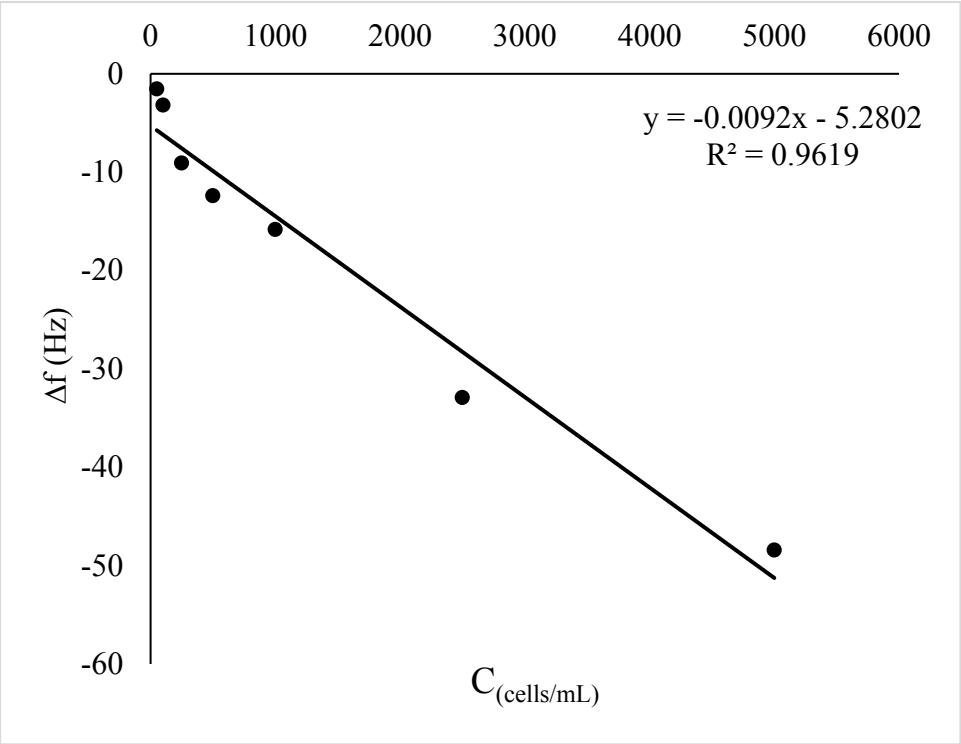

Figure 4. 10. The change in (f) of Ab-NPs QCM chip by A375 cell binding.

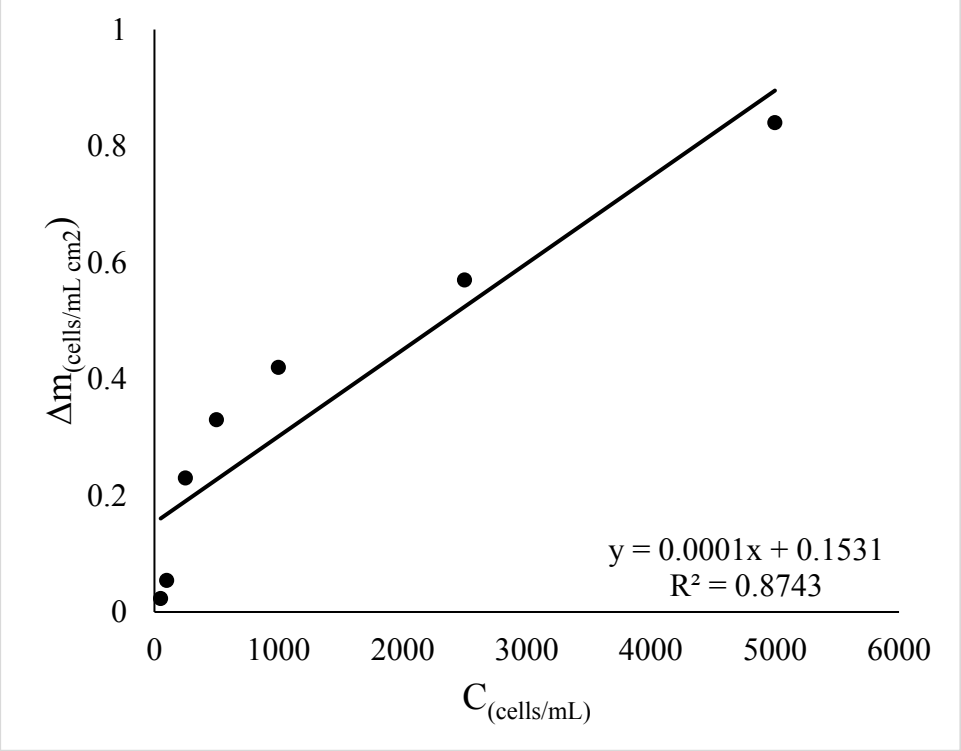

Figure 4. 11. The change in mass (Δm) of Ab-NPs QCM chip by A375 cell binding.

The limit of detection (LOD) and limit of quantification (LOQ) value were determined using data obtained by passaged A375 cells at different concentrations. They were calculated by equation (2) and (3):

$$LOQ = 10* S/m \quad \text{.....(2)}$$

$$LOD = 3.3* S/m \quad \text{.....(3)}$$

m represents the slope of the curve and S represents the standard deviation. This indicates that the QCM biosensor detects A375 cell quantitatively. The LOD is the lowest concentration of the substance to be detected under specific conditions. While the LOQ is the lowest concentration of the substance to be detected under certain conditions. LOD and LOQ were measured based on the slope and standard deviation of the curve of change in mass (Δm) values obtained in this study (Figure 4.11). The values were 1.2 cells/mL and 3.6 cells/mL, respectively, and were calculated using Equation (2) and (3).

4.4. Equilibrium Analysis

All concentration values, excluding ($[B]_0$) the total ligand quantity which represents the maximum analyte binding capacity of the surface, can be interpreted as QCM signals. Hence, there is no requirement to convert (m) into (C). Under conditions where the concentration of free analyte remains constant within the flow cell, the binding can be expressed as:

$$d\Delta m/dt = k_a*C*\Delta m_{max} - (k_a*C+k_d)\Delta m \quad \text{.....(4)}$$

Here, $d\Delta m/dt$ represents the rate of concentration change of the QCM signal; m and Δm_{maks} represent the maximum signal measured due to binding and resulting mass increase (cells/mLcm^2); C is the analyte concentration (cells/mL); k_a is the association rate constant (cells/mLs), and k_d is the dissociation rate constant (1/s). The binding constant K_A (cells/mL) is calculated from the ratio of k_a to k_d ($K_A = k_a / k_d$). In the equilibrium state, simplifying the equations is achieved by setting $d\Delta m/dt = 0$:

$$\Delta m/C = K_A*\Delta m_{max} - K_A*\Delta m \quad \text{.....(5)}$$

Therefore, the binding constant K_A is calculated from the Δm / C ratio against the Δm equilibrium graph. The dissociation constant K_D can be calculated using the equation $1/K_A$ as shown in the Figure 4.12.

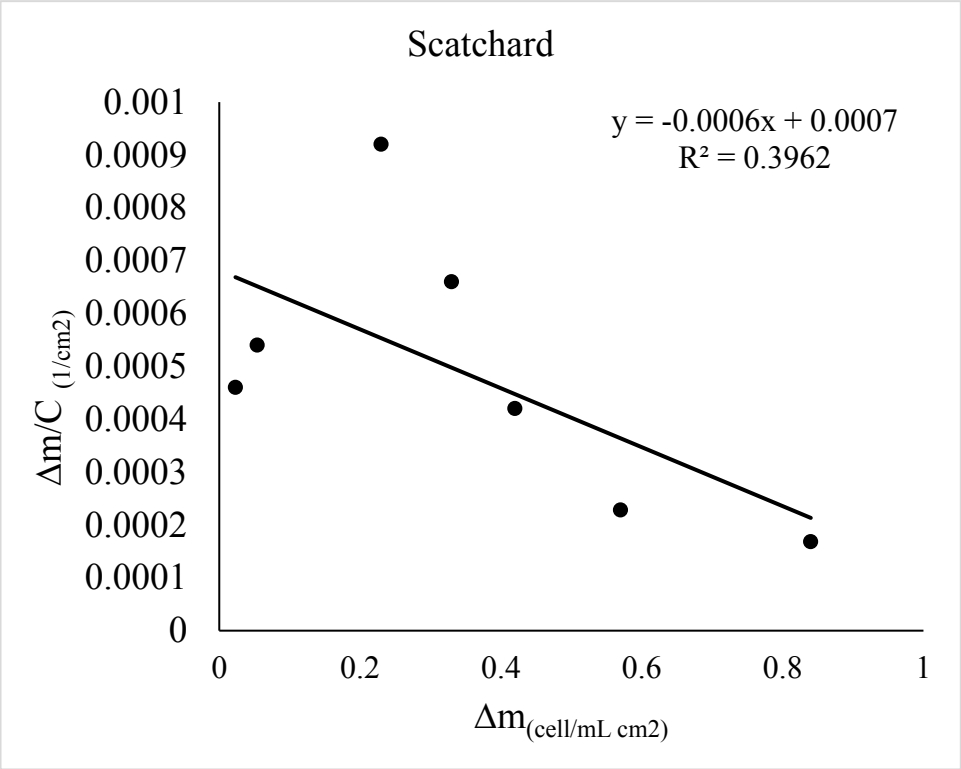

Figure 4. 12. Determination of kinetic rate constants. Equilibrium analysis approach (Scatchard).

4.5. Equilibrium Isotherm Models

Various isotherm models were employed in order to determine the best model for binding between A375 cells and Ab-NPs QCM chip. Scarthard, Langmuir, Freundlich, and Langmuir-Freundlich (LF) models.

Scarthard $\Delta m/C = K_A(\Delta m_{max} - \Delta m)$

Langmuir $\Delta m = \Delta m_{max} * C / K_D + (C)$

Freundlich $\Delta m = \Delta m_{max} * (C)^{1/n}$

Langmuir-Freundlich $\Delta m = \Delta m_{max}(C)^{1/n} / K_D + (C)^{1/n}$

Here, C (cells/mL) represents the cell concentration and Δm (cells/cm^2) the increase in mass per unit area, k_d (s^{-1}) and k_a (cells/ mL) are the backward and forward rate constants

for the reaction. While the K_D (mL/cells) and K_A (cells/mL) represent the reverse and forward equilibrium constants and the Freundlich exponent, denoted as 1/n. Using the changes in mass obtained when passing increasing concentrations of cells on the QCM, equilibrium kinetic analysis was performed and the unknown values in the equations were calculated.

The difference between these models is the nature of the association between the molecule and the surface, whether it is homogeneous or heterogeneous. Freundlich represents heterogeneous adsorption, while Langmuir represents homogeneous adsorption. In Figure 4.13, (A) graph for the Langmuir, (B) for Freundlich, and (C) Langmuir-Freundlich models are provided

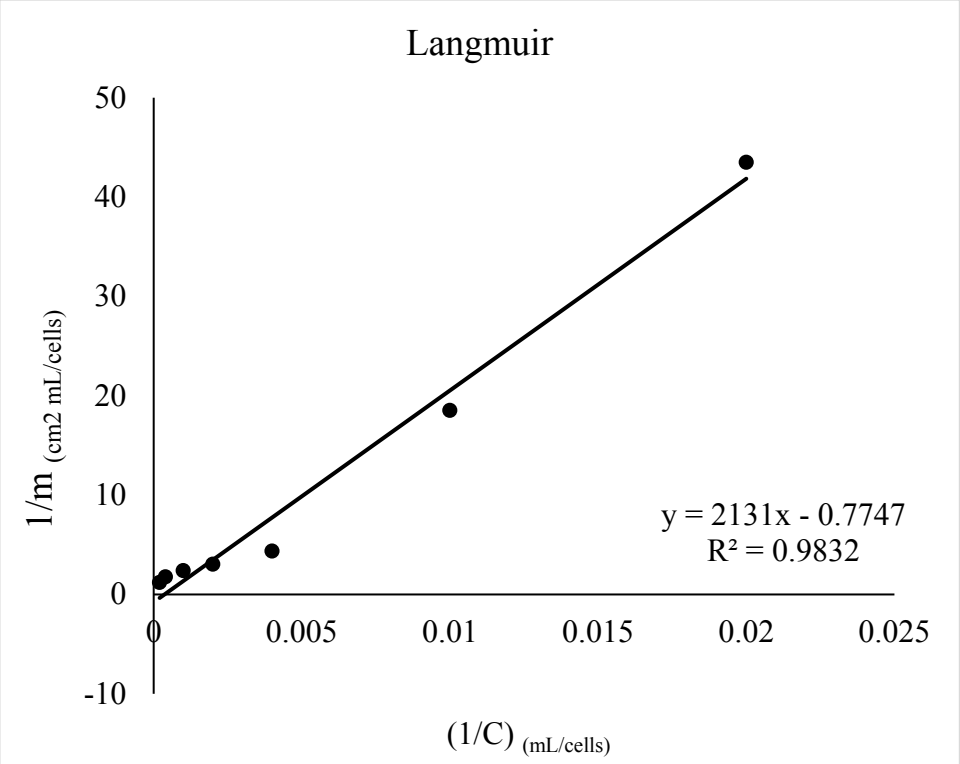

(A)

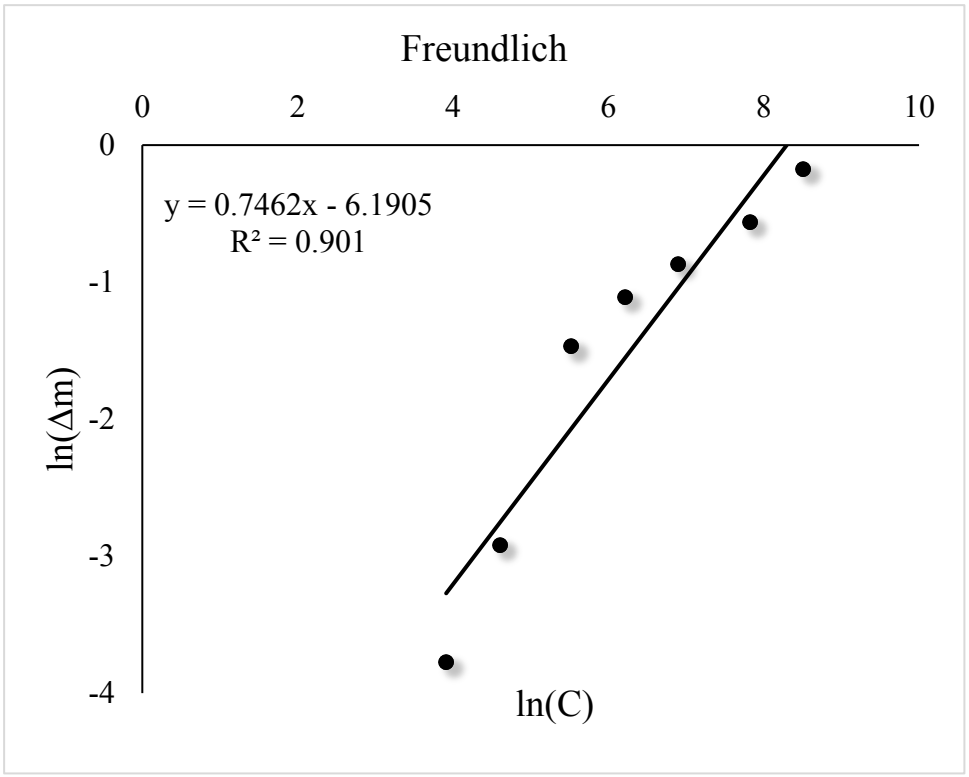

(B)

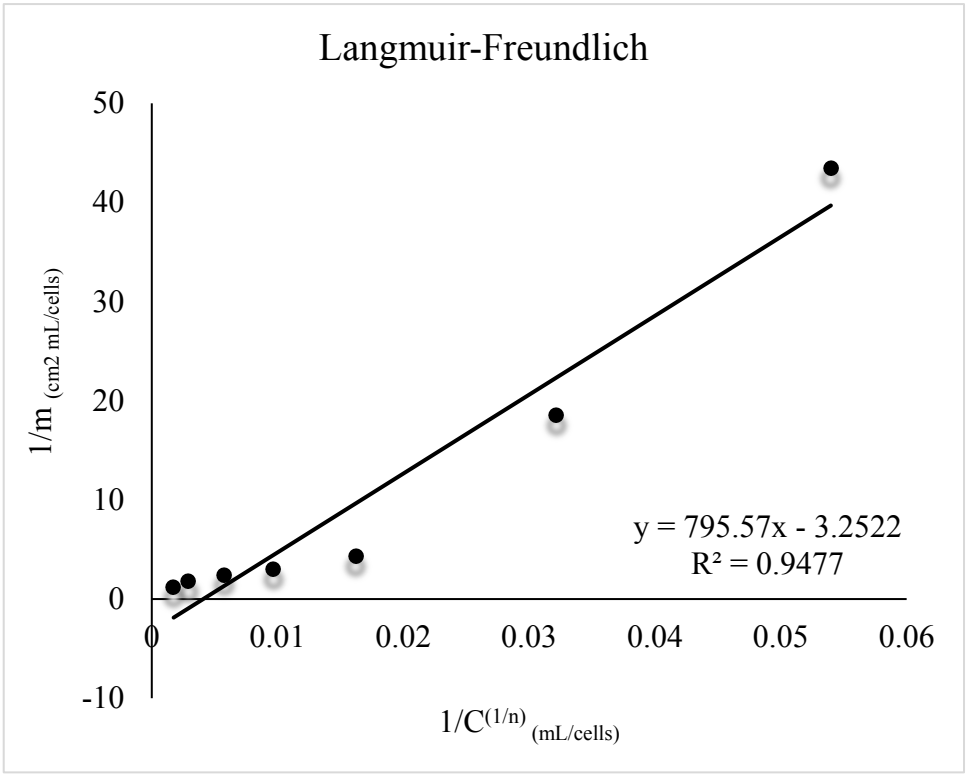

(C)

Figure 4. 13. Adsorption models. (A)Langmuir; (B)Freundlich; (C)Langmuir-Freundlich.

Table 4. 2. Langmuir, Freundlich, and Langmuir-Freundlich parameters.

Langmuir	Freundlich	Langmuir-Freundlich
Δm_{max} = 1.29	Δm_{max} = 2.10897	Δm_{max} = 0.3074
K_A = 0.00036 cells/mL	1/n = 0.7462	1/n = 0.7462
K_D = 2750.74 mL/cells	R^2 =0.901	K_A = 0.004 cells/mL
R^2 =0.9832		K_D = 244.6 mL/cells
		R^2 =0.904

According to the data experimentally obtained in Figure 4.15 and Table 4.2, it is found that the Langmuir model is compatible (R^2 = 0.9832). Interactions between cells are highly homogeneous. This model demonstrates suitability for cells. This adsorption model is highly compatible for cells at both low and high concentrations.

4.6. Competitive Kinetic Analyses

The selectivity coefficients for A375, PANC-1 and HEK294 cell line were determined using the following equation:

$$K_d = [(C_i - C_f)/C_f] \times V/m \quad \text{.....(7)}$$

Where K_d (mL/g) represents the dissociation coefficient; V represents the volume of the solution utilized (mL), C_i and C_f (nM) represent the initial and final concentrations; and m indicates the mass for polymer (g). In QCM sensor applications, the conversion of concentration and mass parameters has been implemented.

This approach is motivated by factors such as the negligible disparity between initial and final concentrations, the challenge in accurately determining the mass of the polymer, and the linear correlation between concentration and Δm. The selectivity coefficient was calculated here based on this equation:

$$k = \Delta m \text{ highly invasive cells} / \Delta m \text{ of invasive cells} \quad \text{.....(8)}$$

To confirm the selectivity of the QCM sensor modified with DF6392 antibody against the A375 cell line, competitive adsorption experiments were performed. Solutions containing A375, HEK294, and PANC-1 cell lines were employed for these investigations. The sensor's reactions to these cell lines are illustrated in the Sensorgram, which depict the relationship between Δf and time, as presented in Figure 4.14.

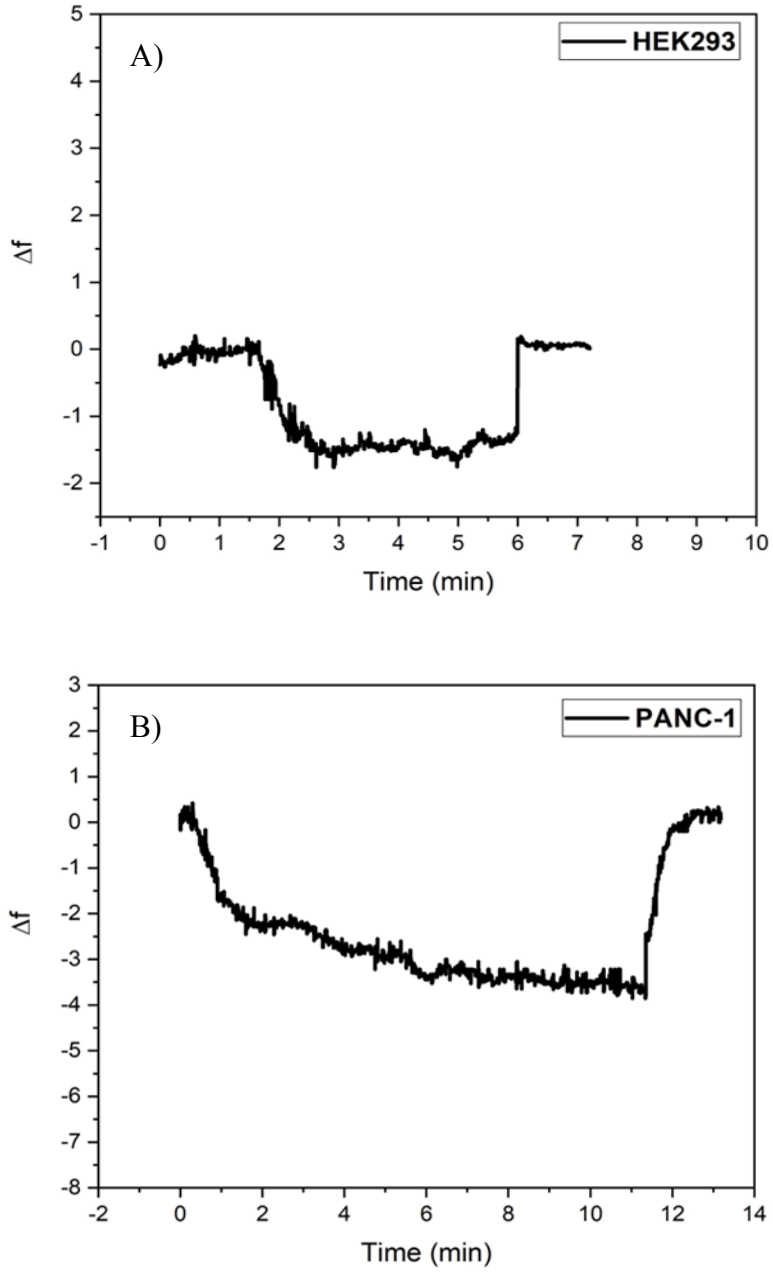

Figure 4. 14. Displays the (change in frequency) (Δf) of the Ab-NPs QCM chip resulting from the binding of HEK294 and PANC-1 cell lines.

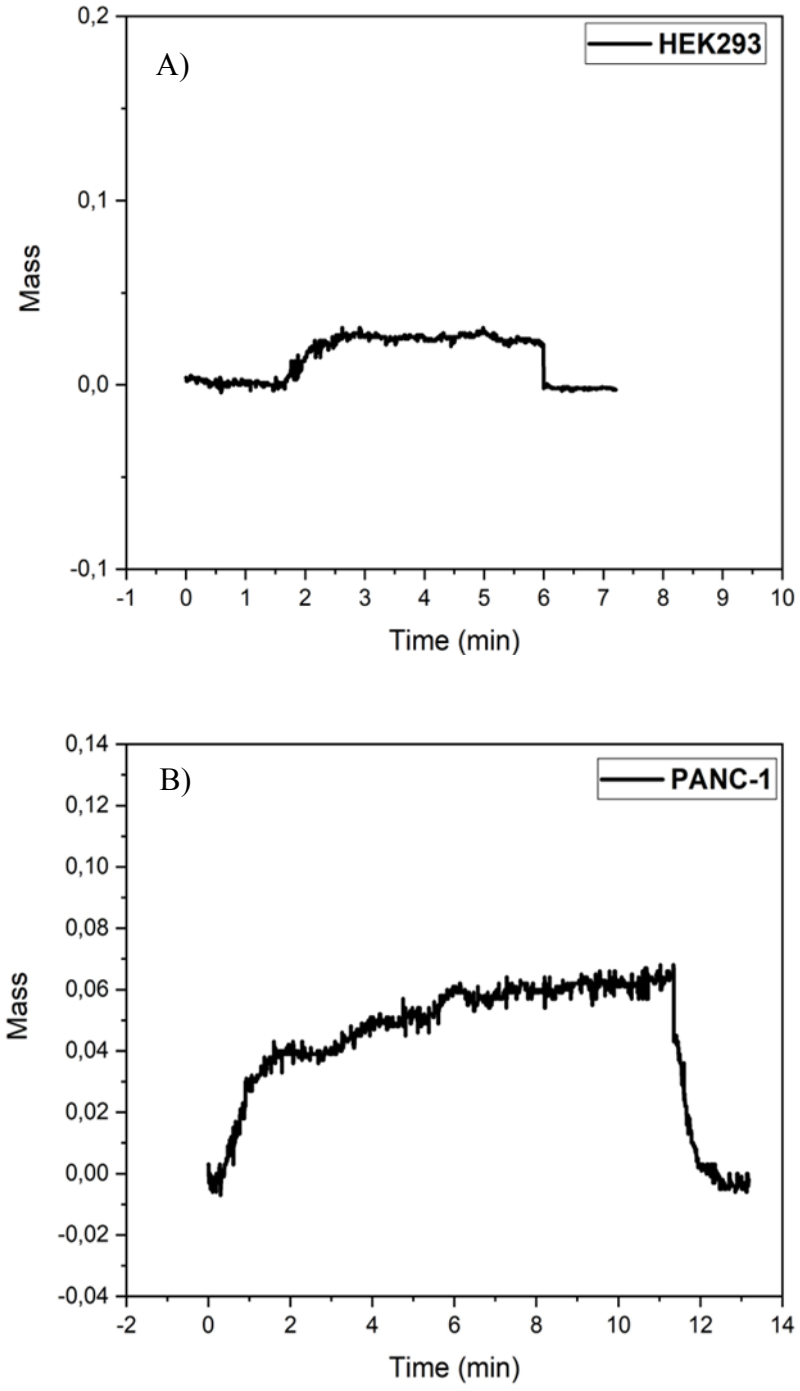

Figure 4. 15. The change in mass on the Ab-NPs QCM chip induced by the binding of (A) HEK294 and (B) PANC-1 cell line binding.

In Figure 4.15. shows the variation in mass per unit area on the surface of the Ab-NPs QCM chip. These results were obtained when the A375, HEK294 and PANC-1 cell lines were passed on the identical Ab-NPs QCM chip, employing the same speed and concentration (2500 cells/mL).

Table 4. 3. Presents the selectivity coefficients (k) for the A375 cell line in comparison to the HEK294 and PANC-1 cell lines.

Cells	Δm	k
A375	0.57	_
HEK294	0.061	09.34
PANC-1	0.024	23.75

Based on these findings, as illustrated in the previous table and Figure 4.16, the Ab-NPs QCM chip demonstrates a detection sensitivity for the A375 cell line that is 9.34 times higher than that for HEK294 and 23.75 times greater than for PANC-1. This heightened sensitivity is attributed to the presence of the CD44 receptor on the surface of HEK294 and PANC-1 cell lines, thereby augmenting the sensor's selectivity. While the CD44 receptor is present on the surface of all three cell types, its abundance is highest in A375, followed by HEK294, with the lowest quantity observed in PANC-1 cells.

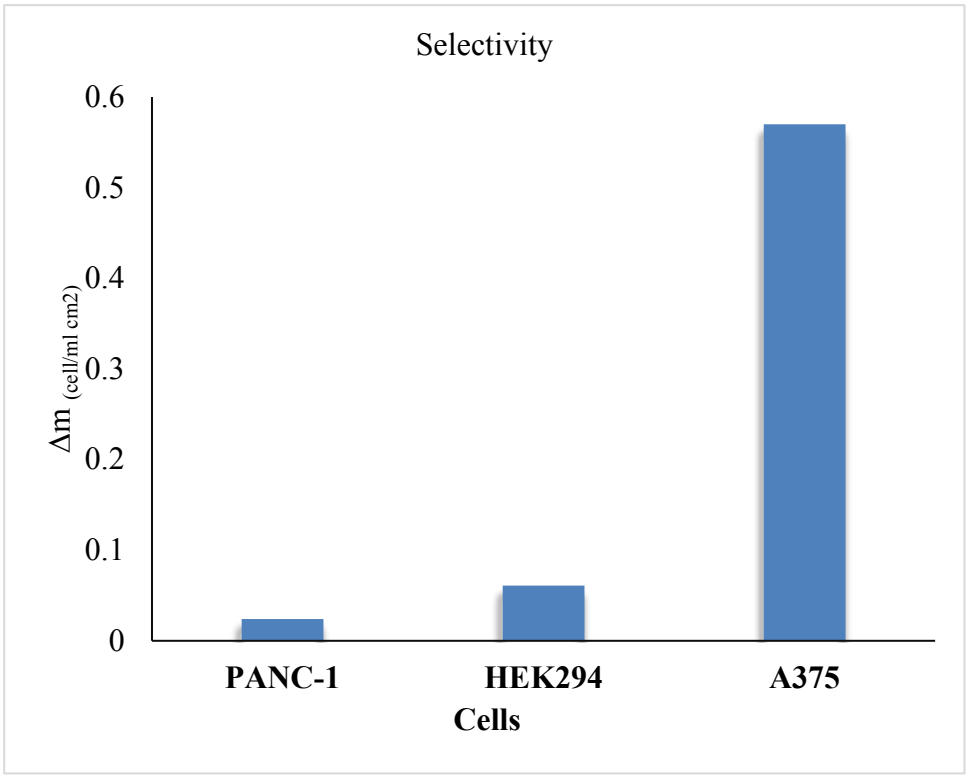

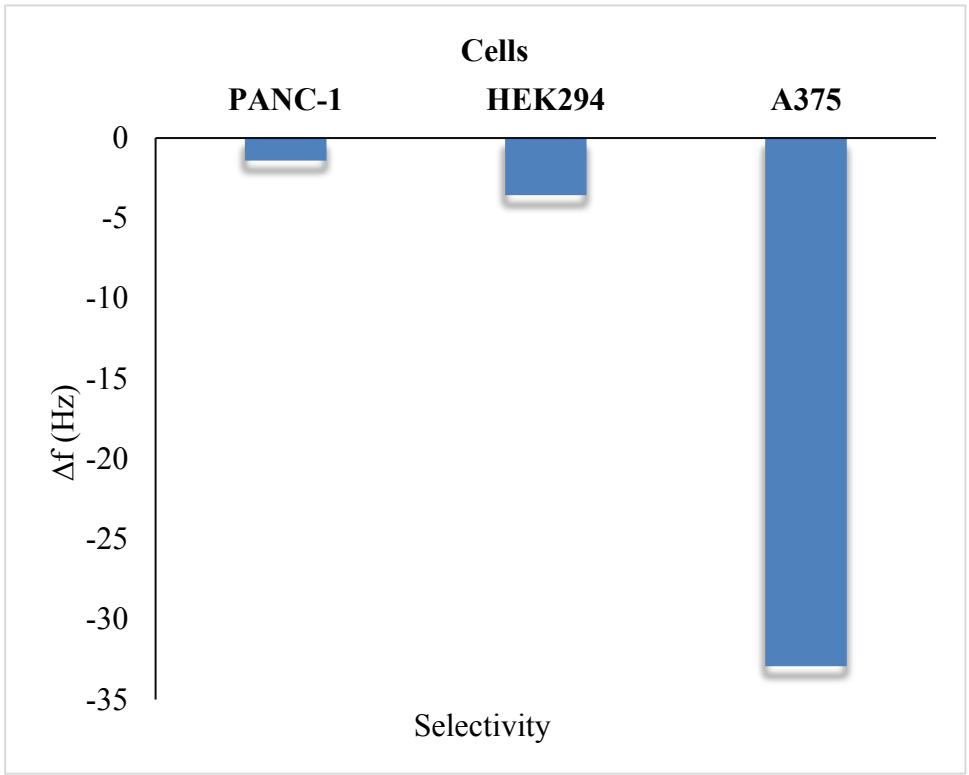

Figure 4. 16. Selectivity of the QCM sensor modified with DF6392 antibody against the A375, HEK294 and PANC-1 cell lines.

4.7. Reusability and Stability Studies

To assess the stability and reusability for Ab-NPs QCM chip, three repetitions of the passage of the same concentration of A375 cells were conducted at the same speed. The recorded change in frequency and mass for each repetition remained constant. This consistent response suggests excellent stability and reusability for Ab-NPs QCM chip over multiple experiments, further validating its reliability in detecting A375 cells.

Over three cycles the binding capacity for modified QCM chip bound to the DF6392 antibody was stable as shown in Figures 4.17 and 4.18. Each analysis was repeated several times using the same QCM chip in all analyses. Which indicates great stability of the QCM chip modified with Ab-NPs. These results demonstrate the possibility of using a QCM chip modified with Ab-NP to detect A375 cells several times without the significant loss in activity because no observable change in QCM signal during these experiments. There was no indication of sensor drift because no chemical reaction occurred that could induce a thermal effect for quartz crystal.

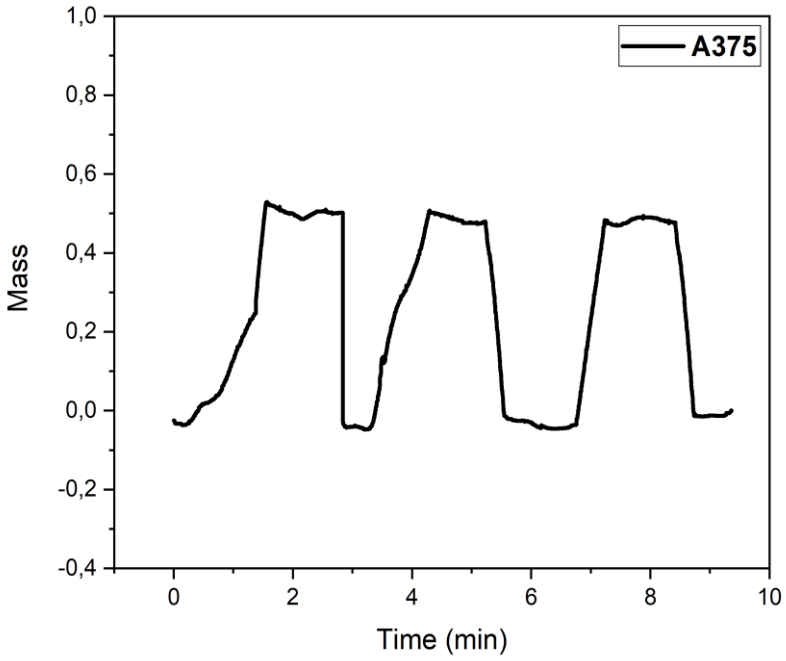

Figure 4. 17. Based on mass changes, performance of Ab-NPs QCM chip in repeated cycles.

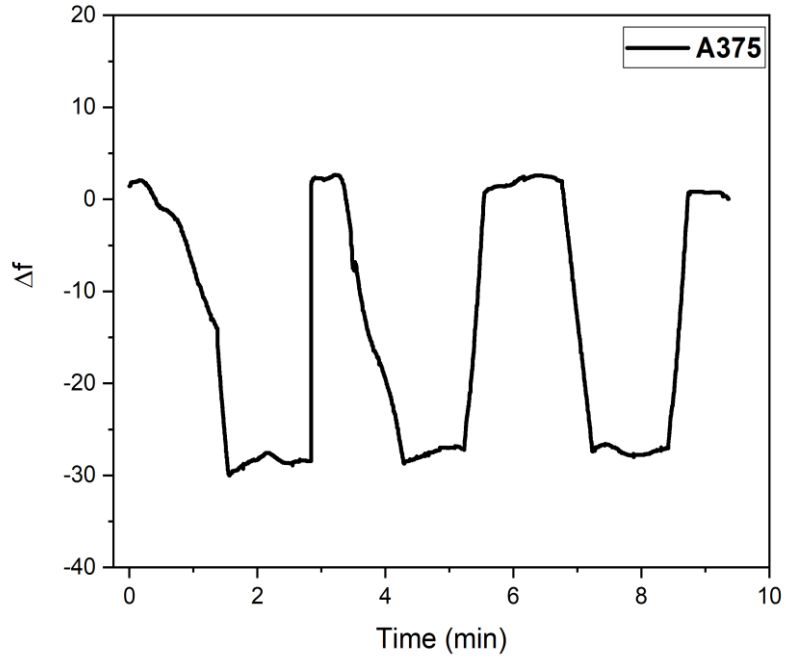

Figure 4. 18. Based on change in frequency (Δf), performance of Ab-NPs QCM chip in repeated cycles.

5. CONCLUSION

- By mini-emulsion polymerization reaction, P(HEMA-NPs) were synthesized using (EDGMA, 98%) and (HEMA, 97%) in order to enhance the surface area for QCM chip.
- P(HEMA-NPs) were characterized by zeta size analysis. The size was determined as 90.29 nm. Its polydispersity was found to be 0.373.
- APTES was employed as a silanization agent to activate the P(HEMA-NPs). Surface modification of the QCM chip was achieved using MUA and EDC/NHS. P(HEMA-NPs)-APTES affixed to the modified QCM chip were modified with DF6392 antibodies.
- FTIR-ATR spectrophotometer was used for characterization P(HEMA-NPs) and P(HEMA-NPs)-APTES. The broad band in the range of 3000 – 3700 cm^{-1} indicated the stretching vibrations of the hydroxyl (-OH) groups in P(HEMA-NPs) decreased with the increasing ($–NH_2$) groups resulting from the modification of the P(HEMA-NPs) with APTES. A new peak in the range of 1000-1100 cm^{-1} refers to a siloxane (Si-O-Si) linkage, indicating the integration of APTES into P(HEMA-NPs) structure. Additionally, appearance of peaks around 3300-3500 cm^{-1} suggested the introduction of amino groups (NH_2), further supporting the successful modification.
- The surface morphology of the unmodified QCM chip, QCM modified with MUA, and MUA-modified QCM with P(HEMA-NPs)-APTES was characterized using AFM. The roughness average of the unmodified QCM chip was determined to be 0.265 nm. It was also determined for the modified QCM chip with MUA and with APTES-P(HEMA-NPs) to be 0.39 nm and 8.18 nm respectively. These results indicate the successful attachment of P(HEMA-NPs)-APTES to the MUA modified gold QCM surface.
- The contact angle measurements conducted on the sensor chip at different stages of modification provided crucial insights into the evolving surface properties. The contact angle value of the unmodified QCM sensor surface was 93.0° ± 1.43°, decreased to 70.6° ± 4.25° when modified with (MUA). Subsequent modification with the APTES-P(HEMA-NPs), induced a substantial decrease to 64.6° ± 4.66°. The final step, involving antibody addition, resulted in a decrease to 39.9° ± 2.65°.

- A notable reduction in the surface contact angle signifies an increase in surface hydrophilicity. This situation can be explained as follows; The P(HEMA-NPs) and MUA have a hydrophilic character because of the presence of carboxylic acid and hydroxyl groups within their structure. For this reason, attaching a hydrophilic group to the surface increased the surface hydrophilicity and decreased the contact angle value. Modifying the P(HEMA-NPs) with APTES increased the hydrophilicity due to siloxane linkages and amino groups. The contact angle value was lower. The amino groups introduced during the APTES modification likely played a crucial role in facilitating specific antibody binding. These systematic decreases in contact angles underscore the successful modification steps.
- A375 cell solutions of different concentrations (50-5000) cells/mL were introduced into the Ab-NPs QCM system one by one (5 mL, flow rate 1 mL/min). The shift values at the Δf and Δm were observed with the increase in concentration of A375 cell solutions. This is because the DF6392 antibody that was placed on the QCM chip binds to CD44 receptors present on the membrane of A375 cells.
- When Δf and Δm versus time graphs are plotted together, the resulting Sensorgram can be examined more easily. It has been clearly determined that as the cell concentration increases, Δf decreases, and Δm also increases.
- The QCM sensor shows linearity in the concentration range (50-5000) cells/mL. When the data evaluated, the equation of the obtained line was calculated as $y = -0.0092x – 5.2802$ and the linearity was calculated as $R^2 = 0.9619$. With this data obtained, the prepared QCM sensor measures with 96.19% linearity in (50-5000) cells/mL.
- It was found that the Langmuir model was the most appropriate. From the Langmuir equation K_A and K_D values were calculated as 0.00036 cells/mL and 2750.74 mL/cell, respectively, and the Δm_{max} value calculated here is 1.29. Interactions between cells are highly homogeneous, demonstrating suitability for cells at both low and high concentrations.
- To confirm the selectivity of the QCM modified with the DF6392 antibody against the A375 cell line, competitive adsorption experiments were performed. Solutions containing A375, HEK294, and PANC-1 cell lines were employed for these investigations at the same speed and concentration. The Sensorgram signal values (Δm) given by Ab-NPs QCM chip surface to A375, HEK294, and PANC-1 cells

are 0.57, 0.061 and 0.024 respectively. Based on these findings, the Ab-NPs QCM chip exhibits a detection sensitivity for the A375 cell line that is 9.34 times greater than that for HEK294 and 23.75 times more pronounced than for PANC-1. This heightened sensitivity is attributed to the presence of the CD44 receptor on the surface of HEK294 and PANC-1 cell lines, thereby augmenting the sensor's selectivity. While the CD44 receptor is present on the surface of all three cell types, its abundance is highest in A375, followed by HEK294, with the lowest quantity observed in PANC-1 cells.

- The selectivity coefficients calculated using Equations 6 were found to be 9.34 for HEK294 and 23.75 for PANC-1.
- To assess the stability and reusability for Ab-NPs QCM chip, three repetitions of the passage of the same concentration of A375 cells were conducted at the same speed. The recorded change in frequency and mass for each repetition remained constant. This consistent response suggests excellent stability and reusability for Ab-NPs QCM chip over multiple experiments, further validating its reliability in detecting A375 cells.

6. RESOURCES

1. Sung, H., et al., *Global cancer statistics 2020: Globocan estimates of incidence and mortality worldwide for 36 cancers in 185 countries.* Ca-a Cancer Journal for Clinicians, 2021. **71**(3): p. 209-249.
2. Jimbow, K., et al., *Mitotic-activity in non-neoplastic melanocytes invivo as determined by histochemical, autoradiographic, and electron-microscope studies.* Journal of Cell Biology, 1975. **66**(3): p. 663-670.
3. Shain, A.H., et al., *The Genetic Evolution of Melanoma from Precursor Lesions.* New England Journal of Medicine, 2015. **373**(20): p. 1926-1936.
4. Gandini, S., P. Autier, and M. Boniol, *Reviews on sun exposure and artificial light and melanoma.* Progress in Biophysics & Molecular Biology, 2011. **107**(3): p. 362-366.
5. Jiang, A.J., P.V. Rambhatla, and M.J. Eide, *Socioeconomic and lifestyle factors and melanoma: a systematic review.* British Journal of Dermatology, 2015. **172**(4): p. 885-915.
6. Adler, N.R., et al., *Concordance of somatic mutational profile in multiple primary melanomas.* Pigment Cell & Melanoma Research, 2018. **31**(5): p. 592-603.
7. Kanavy, H.E. and M.R. Gerstenblith, *Ultraviolet radiation and melanoma.* Seminars in Cutaneous Medicine and Surgery, 2011. **30**(4): p. 222-228.
8. Murphy, A.C., M.E. Wechsler, and N.A. Peppas, *Recent advancements in biosensing approaches for screening and diagnostic applications.* Current Opinion in Biomedical Engineering, 2021. **19**.
9. Rong, G.X., S.R. Corrie, and H.A. Clark, *In vivo biosensing: progress and perspectives.* Acs Sensors, 2017. **2**(3): p. 327-338.
10. Rovira, J. and J.L. Domingo, *Human health risks due to exposure to inorganic and organic chemicals from textiles: A review.* Environmental Research, 2019. **168**: p. 62-69.
11. Vajhadin, F., et al., *Electrochemical cytosensors for detection of breast cancer cells.* Biosensors & Bioelectronics, 2020. **151**.
12. Yang, X.J., et al., *A CD44-biosensor for evaluating metastatic potential of breast cancer cells based on quartz crystal microbalance.* Science Bulletin, 2017. **62**(13): p. 923-930.

13. Seenivasan, R., et al., *An electrochemical immunosensing method for detecting melanoma cells.* Biosensors & Bioelectronics, 2015. **68**: p. 508-515.

14. Untiveros, G., et al., *Normal skin cells increase aggressiveness of cutaneous melanoma by promoting epithelial-to-mesenchymal transition via nodal and wnt activity.* International Journal of Molecular Sciences, 2021. **22**(21).

15. Ernst, M. and A. Giubellino, *The current state of treatment and future directions in cutaneous Malignant Melanoma.* Biomedicines, 2022. **10**(4).

16. Sang, Y.Q. and Y. Deng, *Current insights into the epigenetic mechanisms of skin cancer.* Dermatologic Therapy, 2019. **32**(4).

17. Scolyer, R.A., G.V. Long, and J.F. Thompson, *Evolving concepts in melanoma classification and their relevance to multidisciplinary melanoma patient care.* Molecular Oncology, 2011. **5**(2): p. 124-136.

18. Olbryt, M., *Molecular background of skin melanoma development and progression: therapeutic implications.* Postepy Dermatologii I Alergologii, 2019. **36**(2): p. 129-138.

19. Kozyra, P., D. Krasowska, and M. Pitucha, *New potential agents for malignant melanoma treatment-most recent studies 2020-2022.* International Journal of Molecular Sciences, 2022. **23**(11).

20. Kang, Y.T., et al., *Isolation of circulating tumor cells to diagnose melanoma and evaluate the efficacy of surgical resection using melanoma-specific microsystem.* Advanced Nanobiomed Research, 2022. **2**(8).

21. Mao, L.L., et al., *Immunotherapy in acral and mucosal melanoma: current status and future directions.* Frontiers in Immunology, 2021. **12**.

22. Hershko, D.D., et al., *Sentinel lymph node biopsy in thin melanoma patients.* Journal of Surgical Oncology, 2006. **93**(4): p. 279-285.

23. Keung, E.Z. and J.E. Gershenwald, *The eighth edition American Joint Committee on Cancer (AJCC) melanoma staging system: implications for melanoma treatment and care.* Expert Review of Anticancer Therapy, 2018. **18**(8): p. 775-784.

24. Arnold, M., et al., *Global Burden of Cutaneous Melanoma in 2020 and Projections to 2040.* Jama Dermatology, 2022. **158**(5): p. 495-503.

25. Davis, L.E., S.C. Shalin, and A.J. Tackett, *Current state of melanoma diagnosis and treatment.* Cancer Biology & Therapy, 2019. **20**(11): p. 1366-1379.

26. Wada-Ohno, M., T. Ito, and M. Furue, *Adjuvant therapy for melanoma.* Current Treatment Options in Oncology, 2019. **20**(8).

27. Garzón, V., et al., *Optical biosensors for therapeutic drug monitoring.* Biosensors-Basel, 2019. **9**(4).

28. Sullivan, R.J., et al., *An update on the society for immunotherapy of cancer consensus statement on tumor immunotherapy for the treatment of cutaneous melanoma: version 2.0.* Journal for Immunotherapy of Cancer, 2018. **6**.

29. Brandberg, Y., et al., *Psychological effects of participation in a prevention program for individuals with increased risk for malignant-melanoma.* European Journal of Cancer, 1992. **28A**(8-9): p. 1334-1338.

30. Hong, A. and G. Fogarty, *Role of radiation therapy in cutaneous melanoma.* Cancer Journal, 2012. **18**(2): p. 203-207.

31. Dinnes, J., et al., *Dermoscopy, with and without visual inspection, for diagnosing melanoma in adults.* Cochrane Database of Systematic Reviews, 2018(12).

32. Bono, A., et al., *Clinical and dermatoscopic diagnosis of early amelanotic melanoma.* Melanoma Research, 2001. **11**(5): p. 491-494.

33. Kok, Y., et al., *The impact of incomplete clinical information and initial biopsy technique on the histopathological diagnosis of cutaneous melanoma.* Australasian Journal of Dermatology, 2021. **62**(4): p. E524-E531.

34. Pacifico, M.D., et al., *CD44v3 levels in primary cutaneous melanoma are predictive of prognosis: Assessment by the use of tissue microarray.* International Journal of Cancer, 2006. **118**(6): p. 1460-1464.

35. Kudrin, K.G., et al., *Early diagnosis of skin melanoma using several imaging systems.* Optics and Spectroscopy, 2020. **128**(6): p. 824-834.

36. Azoury, S.C. and J.R. Lange, *Epidemiology, risk factors, prevention, and early detection of melanoma.* Surgical Clinics of North America, 2014. **94**(5): p. 945-+.

37. Feit, N.E., S.W. Dusza, and A.A. Marghoob, *Melanomas detected with the aid of total cutaneous photography.* British Journal of Dermatology, 2004. **150**(4): p. 706-714.

38. Guo, Q., C.X. Yang, and F. Gao, *The state of CD44 activation in cancer progression and therapeutic targeting.* Febs Journal, 2022. **289**(24): p. 7970-7986.

39. Serra, M., et al., *Differential expression of CD44 in canine melanocytic tumours.* Journal of Comparative Pathology, 2004. **130**(2-3): p. 171-180.

40. Weigel, M.T. and M. Dowsett, *Current and emerging biomarkers in breast cancer: prognosis and prediction.* Endocrine-Related Cancer, 2010. **17**(4): p. R245-R262.

41. Ahrens, T., et al., *CD44 is the principal mediator of hyaluronic-acid-induced melanoma cell proliferation.* Journal of Investigative Dermatology, 2001. **116**(1): p. 93-101.

42. Ota, T., et al., *CD44 participates in tumor-cell adhesion to endothelial-cells in the experimental metastatic process in b16bl6 melanoma-cells.* Anticancer Research, 1995. **15**(4): p. 1215-1219.

43. Dou, J., et al., *Overexpression of microrna-200c in cd44+cd133+cscs inhibits the cellular migratory and invasion as well as tumorigenicity in mice.* Cellular and Molecular Biology, 2013. **59**: p. 1861-1868.

44. Cui, M., et al., *A dual-responsive electrochemical biosensor based on artificial protein imprinted polymers and natural hyaluronic acid for sensitive recognition towards biomarker CD44.* Sensors and Actuators B-Chemical, 2022. **371**.

45. Fattahi, Z., A.Y. Khosroushahi, and M. Hasanzadeh, *Recent progress on developing of plasmon biosensing of tumor biomarkers: Efficient method towards early stage recognition of cancer.* Biomedicine & Pharmacotherapy, 2020. **132**.

46. Zhou, B., et al., *Real-time quartz crystal microbalance cytosensor based on a signal recovery strategy for in-situ and continuous monitoring of multiple cell membrane glycoproteins.* Biosensors & Bioelectronics, 2018. **111**: p. 90-96.

47. Saylan, Y., et al., *Detecting Fingerprints of Waterborne Bacteria on a Sensor.* Chemosensors, 2019. **7**(3).

48. Idil, N., et al., *Whole cell based microcontact imprinted capacitive biosensor for the detection of Escherichia coli.* Biosensors & Bioelectronics, 2017. **87**: p. 807-815.

49. Wang, J., *Electrochemical biosensors: Towards point-of-care cancer diagnostics.* Biosensors & Bioelectronics, 2006. **21**(10): p. 1887-1892.

50. Bunde, R.L., E.J. Jarvi, and J.J. Rosentreter, *Piezoelectric quartz crystal biosensors.* Talanta, 1998. **46**(6): p. 1223-1236.

51. Bahadir, E.B. and M.K. Sezgintürk, *Electrochemical biosensors for hormone analyses.* Biosensors & Bioelectronics, 2015. **68**: p. 62-71.

52. Liu, Y.Q., L. Yang, and Y. Cui, *Transdermal amperometric biosensors for continuous glucose monitoring in diabetes.* Talanta, 2023. **253**.

53. Kaur, B., S. Kumar, and B.K. Kaushik, *Recent advancements in optical biosensors for cancer detection.* Biosensors & Bioelectronics, 2022. **197**.

54. Diltemiz, S.E., et al., *Molecular imprinting technology in quartz crystal microbalance (QCM) sensors.* Sensors, 2017. **17**(3).

55. Akgönüllü, S., et al., *Rapid and sensitive detection of synthetic cannabinoids JWH-018, JWH-073 and their metabolites using molecularly imprinted polymer-coated QCM nanosensor in artificial saliva.* Microchemical Journal, 2020. **153**.

56. Adamczyk, Z., M. Sadowska, and P. Zeliszewska, *Applicability of QCM-D for quantitative measurements of nano- and microparticle deposition kinetics: theoretical modeling and experiments.* Analytical Chemistry, 2020. **92**(22): p. 15087-15095.

57. Bakhshpour, M., et al., *Quartz crystal microbalance biosensor for label-free MDA MB 231 cancer cell detection via notch-4 receptor.* Talanta, 2019. **204**: p. 840-845.

58. Wu, Y.Q., et al., *Construction of self-assembled polyelectrolyte/cationic microgel multilayers and their interaction with anionic dyes using quartz crystal microbalance and atomic force microscopy.* Acs Omega, 2021. **6**(8): p. 5764-5774.

59. Tothill, I.E., *Biosensors for cancer markers diagnosis.* Seminars in Cell & Developmental Biology, 2009. **20**(1): p. 55-62.

60. Bakhshpour, M., et al., *Microcontact imprinted quartz crystal microbalance nanosensor for protein C recognition.* Colloids and Surfaces B-Biointerfaces, 2017. **151**: p. 264-270.

61. Ogi, H., *Wireless-electrodeless quartz-crystal-microbalance biosensors for studying interactions among biomolecules: A review.* Proceedings of the Japan Academy Series B-Physical and Biological Sciences, 2013. **89**(9): p. 401-417.

62. Wang, Y., et al., *A carbon single crystal electrode for an electrochemical quartz crystal microbalance study.* Journal of Electroanalytical Chemistry, 1996. **419**(1): p. 1-6.

63. Ecker, R., et al., *Design of a dual electrochemical quartz crystal microbalance with dissipation monitoring.* Journal of Sensors and Sensor Systems, 2022. **11**(1): p. 21-28.

64. Taguchi, M. and H. Sugita, *Analysis for electrolytic oxidation and reduction of $PbSO_4$ Pb electrode by electrochemical QCM technique.* Journal of Power Sources, 2002. **109**(2): p. 294-300.

65. Vaughan, R.D., C.K. O'Sullivan, and G.G. Guilbault, *Sulfur based self-assembled monolayers (SAM's) on piezoelectric crystals for immunosensor development.* Fresenius Journal of Analytical Chemistry, 1999. **364**(1-2): p. 54-57.

66. Zeng, X.Q. and R. Mernaugh, *Single-Chain fragment variable recombinant antibodies and their applications in biosensors for cancer diagnosis*. Biosensors and Cancer, ed. V.R. Preedy and V.B. Patel. 2013. 337-358.

67. Arif, S., et al., *Blueprint of quartz crystal microbalance biosensor for early detection of breast cancer through salivary autoantibodies against ATP6AP1.* Biosensors & Bioelectronics, 2015. **65**: p. 62-70.

68. Lim, J.Y. and S.S. Lee, *Sensitive detection of microRNA using QCM biosensors: sandwich hybridization and signal amplification by TiO_2 nanoparticles.* Analytical Methods, 2020. **12**(42): p. 5103-5109.

69. Yilmaz, M., et al., *Quartz crystal microbalance (QCM) based biosensor functionalized by her2/neu antibody for breast cancer cell detection.* Chemosensors, 2021. **9**(4).

70. Chen, Q., et al., *A fluorescence biosensor for tyrosinase activity analysis based on silicon-doped carbon quantum dots.* Chemical & Pharmaceutical Bulletin, 2023. **71**(11): p. 812-818.

71. Ma, X.G., et al., *Lucigenin fluorescent assay of tyrosinase activity and its inhibitor screening.* Sensors and Actuators B-Chemical, 2019. **280**: p. 41-45.

72. Wang, W.X., et al., *Novel green fluorescent probe stem from carbon quantum dots for specific recognition of tyrosinase in serum and living cells.* Journal of Fluorescence, 2023. **33**(2): p. 739-750.

73. Ye, S., et al., *Electrochemical immunoassay of melanoma biomarker cpeb4 based on cobalt porphyrin functionalized graphene oxide.* Journal of the Electrochemical Society, 2022. **169**(2).

74. Gündogdu, A., E.B. Aydin, and M.K. Sezgintürk, *A novel electrochemical immunosensor based on ITO modified by carboxyl-ended silane agent for ultrasensitive detection of MAGE-1 in human serum.* Analytical Biochemistry, 2017. **537**: p. 84-92.

75. Demirbakan, B. and M.K. Sezgintürk, *A sensitive and disposable indium tin oxide based electrochemical immunosensor for label-free detection of MAGE-1.* Talanta, 2017. **169**: p. 163-169.

76. Xue, Y.R., et al., *Quantifying thiol-gold interactions towards the efficient strength control.* Nature Communications, 2014. **5**.

77. Hermanson, G.T., *Bioconjugate techniques, 3rd edition*. Bioconjugate Techniques, 3rd Edition. 2013. 1-1146.

78. Tsai, T.C., et al., *In situ study of EDC/NHS immobilization on gold surface based on attenuated total reflection surface-enhanced infrared absorption spectroscopy (ATR-SEIRAS).* Colloids and Surfaces B-Biointerfaces, 2019. **175**: p. 300-305.

79. Kuru, C.I., et al., *Preparation and characterization of silanized poly(HEMA) nanoparticles for recognition of sugars.* Artificial Cells Nanomedicine and Biotechnology, 2016. **44**(3): p. 835-841.

80. Deepa, N., et al., *Suitability of PEG capped carboxylic acid terminated fluorescent ZnS nanoparticles for NDV peptide binding.* Applied Nanoscience, 2021. **11**(8): p. 2337-2346.

81. Larkin, P. J., *IR and Raman Spectroscopy: Principles and Spectral Interpretation.* Elsevier, 2018.